EUROPEAN ORGANIZATION FOR NUCLEAR RESEARCH

L3 Note 2585
June 30, 2000

Search for R-parity Violating Supersymmetry in e^+e^- Collisions at $\sqrt{s} = 189$–202 GeV

The L3 Collaboration

Abstract

A search for chargino, neutralino and scalar lepton pair production in e^+e^- collisions at the center-of-mass energy between 189 GeV and 202 GeV is performed under the assumptions that R-parity is not conserved and one of the λ_{ijk}, λ'_{ijk} or λ''_{ijk} coupling constants is non-negligible. No signal is found in the data sample. Limits on the production cross sections, on the Minimal Supersymmetric Standard Model parameters and on the masses of the supersymmetric particles are derived. All results are preliminary.

Submitted to the *XXXth International Conference on High Energy Physics*
July 27 - August 2, 2000, Osaka, Japan

1 Introduction

The most general superpotential of the Minimal Supersymmetric Standard Model (MSSM) [1], which describes a supersymmetric, renormalizable and gauge invariant theory, with minimal particle content, includes the term W_R [2,3]:

$$W_R = \lambda_{ijk} L_i L_j \overline{E}_k + \lambda'_{ijk} L_i Q_j \overline{D}_k + \lambda''_{ijk} \overline{U}_i \overline{D}_j \overline{D}_k \, , \qquad (1)$$

where λ_{ijk}, λ'_{ijk} and λ''_{ijk} are the Yukawa couplings and i, j and k the generation indices; L_i and Q_i are the left-handed lepton- and quark-doublet superfields, $\overline{E}_i$, $\overline{D}_i$ and $\overline{U}_i$ are the right-handed singlet superfields for charged leptons, down- and up-type quarks, respectively. In order to prevent the simultaneous presence of identical fermionic fields, the following antisymmetry relations are required: $\lambda_{ijk} = -\lambda_{jik}$ and $\lambda''_{ijk} = -\lambda''_{ikj}$, so that there are in total $9+27+9$ independent Yukawa couplings.

The $L_i L_j \overline{E}_k$ and $L_i Q_j \overline{D}_k$ terms violate the leptonic quantum number L, while the $\overline{U}_i \overline{D}_j \overline{D}_k$ terms violate the baryonic quantum number B. Their simultaneous presence would lead to a fast proton decay [4], which is experimentally excluded [5]. This can be avoided by imposing the conservation of R-parity, a multiplicative quantum number defined as:

$$R = (-1)^{3B+L+2S} \, , \qquad (2)$$

where S is the spin. R is +1 for all ordinary particles, and −1 for their supersymmetric partners. If R-parity is conserved, supersymmetric particles can be produced only in pairs and they decay in cascade to the lightest supersymmetric particle (LSP), which is stable. However, the absence of either the B-violating or the L-violating terms, or of a subset of them, is enough to prevent a fast proton decay. As a consequence, two new kind of processes are allowed: single production of supersymmetric particles or LSP decays into Standard Model particles via scalar lepton or quark exchange. In the latter case, the MSSM production mechanisms are unaltered by the operators in Eq. 1.

In this paper, we search for pair-produced neutralinos ($e^+e^- \to \tilde{\chi}^0_m \tilde{\chi}^0_n$, with $m = 1, 2$ and $n = 1, .., 4$), charginos ($e^+e^- \to \tilde{\chi}^+_1 \tilde{\chi}^-_1$) and scalar leptons ($e^+e^- \to \tilde{\ell}^+_R \tilde{\ell}^-_R$, $e^+e^- \to \tilde{\nu}\tilde{\nu}$) with subsequent R-parity violating decays, assuming that one of the λ_{ijk}, λ'_{ijk} or λ''_{ijk} coupling constants is non-negligible. Supersymmetric particles can decay directly to two or three fermions according to the dominant interaction term, as detailed in Table 1. Indirect decays via the LSP can occur as well. Four-body decays of the lightest scalar lepton are also taken into account in the case of λ''_{ijk}. In the present analysis, the dominant coupling is assumed to be greater than 10^{-5} [6], corresponding to decay lengths smaller than 1 cm. Previous results on λ_{ijk} and λ''_{ijk} Yukawa couplings can be found in Ref. [7]. Searches for R-parity violating decays of supersymmetric particles have also been performed by other LEP experiments [8].

2 Data and Monte Carlo Samples

The data used correspond to an integrated luminosity of 176.4 pb^{-1} collected by the L3 detector [9] at the center-of-mass energy ($\sqrt{s}$) of 189 GeV.

Only λ''_{ijk} analyses have been updated with 1999 data. The data sample corresponds in this case to integrated luminosities of 29.7 pb^{-1}, 83.7 pb^{-1}, 82.8 pb^{-1} and 37.0 pb^{-1}at center-of-mass energies of 192 GeV, 196 GeV, 200 GeV and 202 GeV, respectively. The search for R-parity violating supersymmetry at $\sqrt{s}$ between 192 GeV and 202 GeV is described in Section 9.

Particle	Direct decays			Indirect decays	
	λ_{ijk}	λ'_{ijk}	λ''_{ijk}	via $\tilde{\chi}^0_1$	via $\tilde{\ell}$
$\tilde{\chi}^0_1$	$\ell^-_i\nu_j\ell^+_k$, $\nu_i\ell^+_j\ell^-_k$	$\ell^-_i u_j\bar{d}_k$, $\nu_i d_j\bar{d}_k$	$\bar{u}_i\bar{d}_j\bar{d}_k$	$-$	$\ell\tilde{\ell}$
$\tilde{\chi}^0_{n(n\geq 2)}$	$\ell^-_i\nu_j\ell^+_k$, $\nu_i\ell^+_j\ell^-_k$	$\ell^-_i u_j\bar{d}_k$, $\nu_i d_j\bar{d}_k$	$\bar{u}_i\bar{d}_j\bar{d}_k$	$\mathrm{Z}^*\tilde{\chi}^0_1$, $\mathrm{Z}^*\tilde{\chi}^0_{m(m\leq n)}$, $\mathrm{W}^*\tilde{\chi}^\pm_1$	$\ell\tilde{\ell}$
$\tilde{\chi}^+_1$	$\nu_i\nu_j\ell^+_k$, $\ell^+_i\ell^+_j\ell^-_k$	$\nu_i u_j\bar{d}_k$, $\ell^+_i\bar{d}_j d_k$	$\bar{d}_i\bar{d}_j\bar{d}_k$, $u_i u_j d_k$, $u_i d_j u_k$	$\mathrm{W}^*\tilde{\chi}^0_1$, $\mathrm{W}^*\tilde{\chi}^0_2$	
$\tilde{\ell}^-_{kR}$	$\nu_i\ell^-_j$, $\nu_j\ell^-_i$	$-$	$-$	$\ell_k\tilde{\chi}^0_1$	$-$
$\tilde{\nu}_{iL}$	$\ell^-_j\ell^+_k$	$d_j\bar{d}_k$	$-$	$\nu_i\tilde{\chi}^0_1$	
$\tilde{\nu}_{jL}$	$\ell^-_i\ell^+_k$	$-$	$-$	$\nu_j\tilde{\chi}^0_1$	

Table 1: Allowed R-parity violating decays of the supersymmetric particles. Charged conjugate states are implied. Indirect decays via scalar leptons are relevant only for neutralinos when the scalar lepton is the LSP. Only supersymmetric partners of the right-handed charged leptons are taken into account. Decays to more than three fermions are not listed.

The signal events are generated with SUSYGEN [10] for different mass values and for all possible choices of the generation indices.

The following Monte Carlo generators are used to simulate Standard Model processes: PYTHIA [11] for $\mathrm{e^+e^-} \to \mathrm{q\bar{q}}$, $\mathrm{e^+e^-} \to \mathrm{Z\,e^+e^-}$ and $\mathrm{e^+e^-} \to \mathrm{ZZ}$, BHWIDE [12] for $\mathrm{e^+e^-} \to \mathrm{e^+e^-}$, KORALZ [13] for $\mathrm{e^+e^-} \to \mu^+\mu^-$ and $\mathrm{e^+e^-} \to \tau^+\tau^-$, PHOJET [14] and PYTHIA for $\mathrm{e^+e^-} \to \mathrm{e^+e^-q\bar{q}}$, DIAG36 [15] for $\mathrm{e^+e^-} \to \mathrm{e^+e^-}\ell^+\ell^-$ ($\ell = \mathrm{e}, \mu, \tau$), KORALW [16] for $\mathrm{e^+e^-} \to \mathrm{W^+W^-}$ and EXCALIBUR [17] for $\mathrm{e^+e^-} \to \mathrm{W}^\pm\,\ell^\mp\nu$. The number of simulated events corresponds to at least 50 times the luminosity of the data, except for Bhabha and two-photon processes, where the Monte Carlo samples correspond to approximately 3 times the luminosity.

The detector response is simulated using the GEANT package [18]. It takes into account effects of energy loss, multiple scattering and showering in the detector materials. Hadronic interactions are simulated with the GHEISHA program [19]. Time dependent inefficiencies of the different subdetectors are also taken into account in the simulation procedure.

An electron is defined as an electromagnetic shower, with energy larger than 1 GeV, matched with a track in the central chamber. Muon identification requires a track in the muon chambers matched with a track in the central chamber. Taus are defined as isolated hadronic narrow jets with energy larger than 2 GeV and one to three associated tracks. The tau energy must be contained in a cone of 10° half opening angle around its direction. No additional tracks and no more than two additional calorimetric clusters are required in a cone of 30° half opening angle. The ratio of the energies in the two cones has to be less than 2.0. Remaining clusters and tracks are classified as hadrons. Jets are reconstructed with the DURHAM algorithm [20]. The jet resolution parameter y_{mn} is defined as the y_{cut} value at which the event configuration changes from n to m jets, when using the DURHAM clustering scheme.

3 $\boldsymbol{\lambda_{ijk}}$ Analysis

Table 2 shows the possible topologies arising when the λ_{ijk} couplings dominate. The different final states can be classified into five categories as follows: $4\ell + \not{E}$, multileptons plus possible jets and $\not{E}$, 6ℓ, $2\ell + \not{E}$, 4ℓ. After a common preselection, a dedicated selection is developed for each group, taking into account lepton flavours, particle boosts and W* and Z* decay products. In the case of the 4ℓ topology the $4\ell + \not{E}$ selections are used, as discussed in section 6.2.

Direct decays	Topologies
$\mathrm{e^+e^-} \to \tilde{\chi}^0_m\tilde{\chi}^0_n \to \ \ell\ell\ell\nu\nu$	$4\ \ell + \not{E}$
$\mathrm{e^+e^-} \to \tilde{\chi}^+_1\tilde{\chi}^-_1 \to \ \ell\ell\ell\ell\ell\ell$	$6\ \ell$
$\ell\ell\ell\ell\nu\nu$	$4\ \ell + \not{E}$
$\ell\ell\nu\nu\nu\nu$	$2\ \ell + \not{E}$
$\mathrm{e^+e^-} \to \tilde{\ell}^+_R\tilde{\ell}^-_R \to \ \ell\nu\ell\nu$	$2\ \ell + \not{E}$
$\mathrm{e^+e^-} \to \tilde{\nu}\tilde{\nu} \to \ \ell\ell\ell\ell$	$4\ \ell$
Indirect decays	Topologies
$\mathrm{e^+e^-} \to \tilde{\chi}^0_m\tilde{\chi}^0_{n(n\geq 2)}$	$(\geq 4)\ \ell$ + (jets) + $\not{E}$
$\mathrm{e^+e^-} \to \tilde{\chi}^+_1\tilde{\chi}^-_1 \to \ \tilde{\chi}^0_{1(2)}\tilde{\chi}^0_{1(2)}\mathrm{W^*W^*}$	$(\geq 4)\ \ell$ + (jets) + $\not{E}$
$\mathrm{e^+e^-} \to \tilde{\ell}^+_R\tilde{\ell}^-_R \to \ \ell\ell\ell\ell\ell\ell\nu\nu$	$6\ \ell + \not{E}$
$\mathrm{e^+e^-} \to \tilde{\nu}\tilde{\nu} \to \ \ell\ell\ell\ell\nu\nu\nu\nu$	$4\ \ell + \not{E}$

Table 2: Processes and topologies considered in the λ_{ijk} coupling analysis. $\tilde{\chi}^0_m\tilde{\chi}^0_n$ indicates neutralino pair production with $m = 1, 2$ and $n = 1, .., 4$. $\not{E}$ (missing energy) indicates final state neutrinos escaping detection.

Events are preselected by requiring at least two charged leptons ($N_{e,\mu,\tau}$), to reduce $\mathrm{q\bar{q}}$ events and hadronic $\mathrm{W^+W^-}$ and ZZ decays. Events have to contain at least 3 charged tracks (N_{tracks}) and 4 calorimetric clusters ($N_{clusters}$) in order to remove $\mathrm{e^+e^-} \to \mathrm{e^+e^-}, \mu^+\mu^-$ and purely leptonic $\tau^+\tau^-$ and $\mathrm{W^+W^-}$ decays. Signal events with 3 and 4 charged tracks arise from final states with four charged leptons and missing energy. Therefore in this case the visible energy (E_{vis}) is required to be smaller than 90% of $\sqrt{s}$, in order to reject $\ell^+\ell^-$ events. If the number of tracks is at least 5, the visible energy has to be smaller than 120% of $\sqrt{s}$, so that signal events with six charged leptons are not suppressed. Back-to-back events, in particular $\tau^+\tau^-$, are reduced by requiring y_{34} to be greater than 0.0002. In order to select also low multiplicity signal events belonging to $2\ell + \not{E}$ topologies, events with at least 2 and less than 6 tracks and with at least 2 and less than 15 clusters are not rejected if the visible energy does not exceed 60% of $\sqrt{s}$ and if there are at least two leptonic jets clustered with $y_{cut} = 0.008$ (N_{jets8}). In this case, the preselection requirement on y_{34} is not applied. In addition, for the $2\ell + \not{E}$ topologies, the acollinearity and acoplanarity angles are required to be below 176°. The acollinearity (θ_{acol}) and acoplanarity (θ_{acop}) angles are calculated by forcing hadronic and leptonic objects in every event into exactly two jets with the DURHAM algorithm.

The polar angle (θ_{miss}) of the missing momentum vector is required to be between 15° and 165°. In order to reject cosmic ray interactions, at least one time of flight measurement (N_{scint}) is required to be consistent with the beam crossing. Tagged two-photon interactions are rejected by requiring the sum of the energies measured in the small angle calorimeters between 1.5° and 9.0° ($E_{lum} + E_{alr}$) to be less than 10 GeV. In addition, the visible energy must be greater than 20% of $\sqrt{s}$. Background from two-photon collisions is further reduced by requiring the transverse missing momentum (p_{miss}) to be greater than 7 GeV.

After the preselection is applied, 995 events are selected in the data sample and 984 ± 6 events are expected from Standard Model processes, of which 398 ± 2 from $\mathrm{W^+W^-}$, 136 ± 3 from $\mathrm{W^\pm e^\mp}\nu$ decays and 258 ± 1 from $\mathrm{q\bar{q}}$ events. The signal preselection efficiency for $\mathrm{e^+e^-} \rightarrow \tilde{\chi}^+_1\tilde{\chi}^-_1$, with subsequent chargino indirect decays, is between 75% and 95% for $M_{\tilde{\chi}^\pm_1} = 94$ GeV and 5 GeV $\leq \Delta M \leq 70$ GeV, where ΔM is the mass difference $\Delta M = M_{\tilde{\chi}^\pm_1} - M_{\tilde{\chi}^0_1}$. For chargino direct decays the efficiency is between 50% and 65% for $M_{\tilde{\chi}^\pm_1} \geq 45$ GeV. For $\mathrm{e^+e^-} \rightarrow \tilde{\chi}^0_1\tilde{\chi}^0_1$ the efficiency ranges from 50% to 80% for 20 GeV$\leq M_{\tilde{\chi}^0_1} \leq 94$ GeV. For scalar lepton pair production the preselection efficiency ranges from 50%, for direct decays and $M_{\tilde{\ell}} = 54$ GeV, to 90% in the case of indirect decays, for $M_{\tilde{\ell}} = 94$ GeV and any ΔM. Figure 1 shows the number of leptons, acollinearity, normalised visible energy and $\ln(y_{34})$ distributions after the preselection. The data are in good agreement with the Monte Carlo expectations.

The four groups of final selections are shown in Table 12 to Table 15. In addition to the variables defined above, we apply cuts on the event thrust and on the energy in the electromagnetic (E_{bgo}) and hadronic calorimeters (E_{hcal}) and on the energy (E^ℓ_n) of the n identified leptons. The cut values are chosen in order to maximize the analysis sensitivity, as described in Section 6.

4 λ'_{ijk} Analysis

Table 3 shows the topologies arising when the λ'_{ijk} couplings dominate. The different final states can be classified into five categories as follows: 4 jets $+2\ell$, 4 jets $+\ell + \not{E}$, 4 jets $+ \not{E}$, multijets plus possible lepton(s) and possible missing energy, scalar lepton selections. The quark flavour composition is given by the j and k generation indices of the dominant λ'_{ijk} coupling. After a common preselection, a dedicated selection is developed for each group, taking into account lepton flavours and charge, particle boosts and $\mathrm{W^*}$ and $\mathrm{Z^*}$ decay products.

Direct decays		Topologies
$\mathrm{e^+e^-} \rightarrow \tilde{\chi}^0_m\tilde{\chi}^0_n$	$\rightarrow$ $qqqq$ $\ell\ell$	4 jets + 2 ℓ
	$qqqq$ $\ell\nu$	4 jets + ℓ + $\not{E}$
	$qqqq$ $\nu\nu$	4 jets + $\not{E}$
$\mathrm{e^+e^-} \rightarrow \tilde{\chi}^+_1\tilde{\chi}^-_1$	$\rightarrow$ $qqqq$ $\ell\ell$	4 jets + 2 ℓ
	$qqqq$ $\ell\nu$	4 jets + ℓ + $\not{E}$
	$qqqq$ $\nu\nu$	4 jets + $\not{E}$
Indirect decays		Topologies
$\mathrm{e^+e^-} \rightarrow \tilde{\chi}^0_m\tilde{\chi}^0_{n(n\geq2)}$		($\geq$ 4) jets (+ leptons) (+ $\not{E}$)
$\mathrm{e^+e^-} \rightarrow \tilde{\chi}^+_1\tilde{\chi}^-_1$	$\rightarrow$ $\tilde{\chi}^0_{1(2)}\tilde{\chi}^0_{1(2)}\mathrm{W^*W^*}$	($\geq$ 4) jets (+ leptons) (+ $\not{E}$)
$\mathrm{e^+e^-} \rightarrow \tilde{e}^+_R\tilde{e}^-_R$	$\rightarrow$ $\tilde{\chi}^0_1\tilde{\chi}^0_1$ ee	4 jets + 2–4 ℓ (+ $\not{E}$)

Table 3: Processes and topologies considered in the λ'_{ijk} coupling analysis. For masses below 50 GeV or small ΔM values not all the jets in the event can be resolved. $\tilde{\chi}^0_m\tilde{\chi}^0_n$ indicates neutralino pair production with $m = 1, 2$ and $n = 1, .., 4$. $\not{E}$ (missing energy) indicates final state neutrinos escaping detection.

Events are preselected by requiring at least 4 charged tracks and 5 calorimetric clusters in order to remove $\mathrm{e^+e^-} \rightarrow \mathrm{e^+e^-}, \mu^+\mu^-$ and purely leptonic $\tau^+\tau^-$ and $\mathrm{W^+W^-}$ decays. At least one time of flight measurement is required to be consistent with the beam crossing to reject cosmic ray interactions. We require at least two jets in the event clustered with the DURHAM algorithm with $y_{cut} = 0.008$ (N_{jets8}). The polar angle of the missing momentum has to be between 7° and 173°. Tagged two-photon interactions are rejected by requiring the sum of the energies measured in the small angle calorimeters between 1.5° and 9.0° to be less than 10 GeV. In addition, the visible energy must be greater than 30% of $\sqrt{s}$. Background from two-photon collisions is further reduced by requiring the energy in a cone of 12° half opening angle around the beam axis not to exceed 20% of the total visible energy.

In this analysis no attempt is made to identify quark flavours. However, the efficiency is found to be slightly higher for events containing b-quarks than for event with light quarks. When the generation index $i = 3$, the decay products of the neutralino pair contain $\tau^+\tau^-$, $\tau\nu_\tau$ or $\nu_\tau\bar{\nu}_\tau$. Since taus are selected with lower efficiency with respect to electrons or muons, this choice of the first generation index provides a conservative estimate for the signal efficiency. The lowest selection efficiency is found thus for the choice $\lambda'_{ijk} = \lambda'_{311}$, that will be quoted in the following.

After the preselection is applied, 11099 events are selected in the data sample and 11022 ± 34 events are expected from Standard Model processes, of which 7677 ± 5 events from $\mathrm{q\bar{q}}$, 2481 ± 2 from $\mathrm{W^+W^-}$ decays and 674 ± 18 from $\mathrm{e^+e^-q\bar{q}}$ events. The signal preselection efficiency for $\mathrm{e^+e^-} \rightarrow \tilde{\chi}^+_1\tilde{\chi}^-_1$ is between 60% and 90% for $M_{\tilde{\chi}^\pm_1} = 94$ GeV and 5 GeV $\leq \Delta M \leq 70$ GeV. For $\mathrm{e^+e^-} \rightarrow \tilde{\chi}^0_1\tilde{\chi}^0_1$ the efficiency is between 60% and 95% for any value of the neutralino mass. For scalar electron pair production it ranges from 50% to 80% for $M_{\tilde{e}_R} = 94$ GeV and ΔM greater than 20 GeV. Figure 2 shows the $\ln(y_{34})$, thrust, normalised visible energy and polar angle of the missing momentum distributions after the preselection. The data are in good agreement with the Monte Carlo expectations.

The five groups of final selections are shown in Table 16 to Table 22. In addition to the ones defined above, we apply cuts on the following variables: the energy in a cone of 12° half opening angle around the beam axis (E_{v12}); the sphericity; the probability ($Prob(\chi^2_{WW}, 5)$ or $Prob(\chi^2_{ZZ}, 5)$) that the reconstructed invariant mass, after a 5C fit, is consistent with $\mathrm{W^+W^-}$ or ZZ pair production; the energy (E^ℓ_{20}) in a cone of 20° half opening angle around the direction of the lepton candidate, calculated subtracting the lepton energy; the jet invariant masses (M_{jet1} and M_{jet2}) and the width of the most and of the second energetic jet (W_{jet1} and W_{jet2} respectively). The width of the most (second) energetic jet is defined as p^{jet}_T/E^{jet}_{max} ($p^{jet}_T/E^{jet}_{second}$), where the event is clustered into exactly two jets and p^{jet}_T is the projection of the component cluster momenta onto a plane perpendicular to the axis of the most energetic jet. The cut values are chosen in order to maximize the analysis sensitivity, as described in Section 6.

5 λ''_{ijk} Analysis

Table 4 shows the topologies arising when the λ''_{ijk} couplings dominate. The flavour composition depends on the generation indices. In the case of neutralino and chargino pair production, the different topologies can be classified into two groups: multijets, multijets with leptons and/or missing energy. After a common preselection, dedicated selections are developed for each group, depending on the particle boosts, the ΔM values and the $\mathrm{W^*}$ decay products. The following process is also considered: $\mathrm{e^+e^-} \rightarrow \tilde{\ell}^+_R\tilde{\ell}^-_R \rightarrow qqqqqq\ell^+\ell^-$, for which a third group of selections is performed, taking into account the lepton flavour.

Direct decays	Topologies
$e^+e^- \to \tilde{\chi}^0_m\tilde{\chi}^0_n \to$ $qqqqqq$	6 jets
$e^+e^- \to \tilde{\chi}^+_1\tilde{\chi}^-_1 \to$ $qqqqqq$	6 jets
Indirect decays	**Topologies**
$e^+e^- \to \tilde{\chi}^0_m\tilde{\chi}^0_{n(n\geq 2)} \to qqqqqq\ qq$	8 jets
$qqqqqq\ \ell\ell$	6 jets + 2 ℓ
$qqqqqq\ \nu\nu$	6 jets + $\not{E}$
$e^+e^- \to \tilde{\chi}^+_1\tilde{\chi}^-_1 \to$ $qqqqqq\ qqqq$	10 jets
$qqqqqq\ qq\ell\nu$	8 jets + ℓ + $\not{E}$
$qqqqqq\ \ell\ell\nu\nu$	6 jets + 2 ℓ + $\not{E}$
$e^+e^- \to \tilde{\ell}^+_R\tilde{\ell}^-_R \to$ $qqqqqq\ \ell\ell$	6 jets + 2 ℓ

Table 4: Processes and topologies considered in the λ''_{ijk} coupling analysis. For masses below 50 GeV or small ΔM values not all the jets in the event can be resolved. $\tilde{\chi}^0_m\tilde{\chi}^0_n$ indicates neutralino pair production with $n = 1, 2$ and $m = 1, .., 4$. $\not{E}$ (missing energy) indicates final state neutrinos escaping detection.

The preselection of the λ''_{ijk} analysis aims at selecting well balanced hadronic events. Low multiplicity events, like leptonic Z and W decays, are rejected by requiring at least 13 calorimetric clusters. At least one charged track has to be present. The visible energy has to be greater than 70% of $\sqrt{s}$. The energy imbalances, parallel (E_{par}) and perpendicular (E_{perp}) to the beam direction, are required to be smaller than 20% of the visible energy. For center-of-mass energies above the Z peak a large fraction of background events contains a hard initial state radiation (ISR) photon. Unbalanced events with an ISR photon in the beam pipe are removed by means of the requirement on the parallel energy imbalance. In order to reject events with an ISR photon seen in the detector, the invariant mass of the hadronic system ($\sqrt{s'}$) has to be greater than 80% of $\sqrt{s}$. In order to remove background contributions from two-photon interactions, the energy in a cone of 12° half opening angle around the beam axis must not exceed 30% of the total visible energy. Furthermore, the thrust axis is required to be well contained in the detector with a polar angle (θ_T) between 8° and 172°.

In this analysis no attempt is made to identify quark flavours. However, the efficiency is found to be slightly higher for events containing b-quarks than for events with light quarks. Therefore, only the results obtained by the choice $\lambda''_{ijk} = \lambda''_{212}$ will be quoted, in the next sections. After the preselection is applied, 5492 events are selected in the data sample and 5463 ± 32 are expected from Standard Model processes, of which 3803 ± 30 $q\bar{q}$ and 1431 ± 3 W^+W^- events. The signal preselection efficiencies are between 80% and 90% for neutralino and slepton pair production. The same values are found for $e^+e^- \to \tilde{\chi}^+_1\tilde{\chi}^-_1$ in case of hadronic decays, for all values of ΔM between 4 GeVand 64 GeV. For chargino leptonic decays the efficiency decreases to about 60% for high values of ΔM. Figure 3 shows the $\ln(y_{34})$, thrust, $\ln(y_{45})$ and width of the most energetic jet (W_{jet1}) distributions after the preselection. There is good agreement between data and Monte Carlo expectations.

The three groups of final selections are shown in Table 23 to Table 25. In addition to the variables defined above, we apply cuts on the width of the most and of the second energetic jet and on E^{ℓ}_{20}. The cut values are chosen in order to maximize the analysis sensitivity, as described in Section 6.

6 Analysis Optimization and Selection Efficiencies

Dedicated selections are performed to maximize a priori the analysis sensitivity $1/\sigma_{95}$, using Monte Carlo signal and background events. σ_{95} is given by:

$$\sigma_{95} = \frac{1}{\varepsilon}\sum_{n=0}^{\infty} c_n(b) P_b(n). \tag{3}$$

Here ε is the signal selection efficiency, $P_b(n)$ is the Poisson probability for n events with an expected background of b events and $c_n(b)$ are the 95% C.L. Bayesian upper limits on the signal expectation values.

The final efficiencies are summarized in Tables 5 and 6, for gauginos and scalar lepton R-parity violating decays, respectively.

6.1 Neutralino and chargino decays

For neutralino and chargino decays we discuss only the results obtained for $\lambda_{ijk} = \lambda_{133}$, $\lambda'_{ijk} = \lambda'_{311}$ and $\lambda''_{ijk} = \lambda''_{212}$, since these choices of the generation indices give the lowest selection efficiencies. In this way, the quoted results will be valid for any λ_{ijk}, λ'_{ijk} or λ''_{ijk} coupling, respectively. The final efficiencies are summarized in Table 5.

In the case of direct R-parity violating decays, the efficiencies are estimated for different mass values of the pair-produced supersymmetric particles. For λ_{133} and λ''_{212} mediated decays, the efficiencies increase with increasing lightest neutralino or chargino mass. At high masses, six fermions are expected to be isotropically produced and can be disentangled from W-pair production background events. For low masses, the signal signatures look like back-to-back jet events and the selection efficiencies are smaller due to the dominant background coming from the two-fermion processes. In addition, for the λ_{133} selection the efficiencies obtained for low masses (below 50 GeV) are higher for chargino than for neutralino due to the contribution of the six charged lepton final state. For λ'_{311} the lowest selection efficiency is obtained in the intermediate mass region, where the W^+W^- background cannot be efficiently rejected using the thrust value.

In the case of indirect R-parity violating decays for both charginos and next-to-lightest neutralinos, the efficiencies are estimated for different masses and ΔM ranges. For a chargino mass of 94 GeV the efficiencies decrease with increasing ΔM, for the λ_{133} , λ'_{311} and λ''_{212} analyses. At high ΔM, the signal signatures are very similar to those of W-pair production. For $M_{\tilde{\chi}^0_m} + M_{\tilde{\chi}^0_n} = 188$ GeV, the efficiencies of the process $e^+e^- \to \tilde{\chi}^0_m\tilde{\chi}^0_n$ ($m = 1, 2,\ n = 2, 3, 4$) decrease slightly with increasing ΔM for the λ_{133} and λ''_{212} analyses. In the case of the λ''_{212} coupling, leptons and neutrinos from W^* decays can carry a relevant fraction of the event energy when ΔM is large, leading to lower selection efficiencies.

6.2 Scalar lepton decays via $\boldsymbol{\lambda_{ijk}}$

The selection efficiencies are shown in Table 6. In the case of pair production of scalar charged leptons, followed by direct decays via λ_{ijk}, the final state contains two leptons plus missing energy. The lepton flavours are given by the indices i and j, independently of the value of k, as shown in Table 1. The lowest selection efficiency is found for $\lambda_{ijk} = \lambda_{12k}$. This is due to the fact that the best analysis sensitivity is achieved by selecting events with at least 3 calorimetric clusters and with visible energy below 55% of $\sqrt{s}$ (see Table 13). For this reason, events with

Direct decays		Mass values		
Coupling	Process	M = 5–20 GeV	M = 25–50 GeV	M=55–94 GeV
λ_{133}	$\tilde{\chi}^0_m\tilde{\chi}^0_n$	4%–13%	21%–35%	41%–51%
λ_{133}	$\tilde{\chi}^+_1\tilde{\chi}^-_1$	8%–10%	15%–36%	43%–45%
λ'_{311}	$\tilde{\chi}^0_m\tilde{\chi}^0_n$, $\tilde{\chi}^+_1\tilde{\chi}^-_1$	6%–17%	19%–28%	21%–26%
λ''_{212}	$\tilde{\chi}^0_m\tilde{\chi}^0_n$, $\tilde{\chi}^+_1\tilde{\chi}^-_1$	–	29%–38%	35%–54%
Indirect decays		ΔM values		
Coupling	Process	ΔM = 5–20 GeV	ΔM = 25–50 GeV	ΔM = 55–80 GeV
λ_{133}	$\tilde{\chi}^0_m\tilde{\chi}^0_{n(n\geq2)}$	50%–51%	48%–50%	42%–46%
λ_{133}	$\tilde{\chi}^+_1\tilde{\chi}^-_1$	47%–59%	33%–43%	14%–27%
λ'_{311}	$\tilde{\chi}^+_1\tilde{\chi}^-_1$	25%–28%	29%–30%	17%–23%
λ''_{212}	$\tilde{\chi}^0_m\tilde{\chi}^0_{n(n\geq2)}$	55%–59%	59%–60%	47%–53%
λ''_{212}	$\tilde{\chi}^+_1\tilde{\chi}^-_1$	54%–62%	60%–66%	43%–56%

Table 5: Efficiency ranges at $\sqrt{s}$ = 189 GeV. $\tilde{\chi}^0_m\tilde{\chi}^0_n$ indicates neutralino pair production with $m = 1, 2$ and $n = 1, .., 4$. Direct decays: the lowest mass values considered are $M_{\tilde{\chi}^0_1} = 5$ GeV and $M_{\tilde{\chi}^\pm_1} = 15$ GeV for λ_{133}, $M = 15$ GeV for λ'_{311} and $M = 45$ GeV for λ''_{212}. For direct neutralino decays via λ_{133} coupling we quote the $\tilde{\chi}^0_1\tilde{\chi}^0_1$ efficiencies. Indirect decays: the chargino selection efficiencies correspond to $M_{\tilde{\chi}^\pm_1} = 94$ GeV. For the process $\tilde{\chi}^0_m\tilde{\chi}^0_n$ the efficiencies correspond to $M_{\tilde{\chi}^0_m} + M_{\tilde{\chi}^0_n} =$ 188 GeV.

lower multiplicity coming from λ_{12k} mediated decays are selected with lower efficiency. The efficiency increases with increasing scalar lepton mass.

In the case of scalar neutrino pair production, four leptons are produced in the final state. For this final state we have used the $4\ell + \not{E}$ and $(\geq 4)\ \ell+$ (jets) $+\not{E}$ selections, without developing a dedicated one. For this reason, events with scalar neutrino decays into electrons and muons are selected with lower efficiency than events with decays into taus. In particular, the smallest efficiency is obtained for λ_{121}, which can give rise to the decays $\tilde{\nu}_e \to \mu^- e^+$ and $\tilde{\nu}_\mu \to e^- e^+$. This effect is due to the selection requirements on the energy in the electromagnetic calorimeter, which are optimized for selecting events with $4\ell + \not{E}$.

Indirect decays of charged scalar leptons ($\tilde{\ell}^+_R\tilde{\ell}^-_R \to \ell^+\ell^-\tilde{\chi}^0_1\tilde{\chi}^0_1$) provide six leptons plus missing energy in the final state. The events are selected by means of the $(\geq 4)\ \ell+$ (jets) $+\not{E}$ selections. Table 6 shows the efficiencies for scalar electron, muon and tau pair production, for different values of $\Delta M = M_{\tilde{\ell}_R} - M_{\tilde{\chi}^0_1}$. For large values of ΔM the selection efficiencies are smaller for $\tilde{e}^+_R\tilde{e}^-_R$ than for the other channels because of the cut on E_{bgo}.

Indirect decays of scalar neutrinos ($\tilde{\nu}\tilde{\nu} \to \nu\nu\tilde{\chi}^0_1\tilde{\chi}^0_1$) are selected by the $4\ell + \not{E}$ selections. The efficiency decreases with increasing ΔM, when the two additional neutrinos can carry a relevant fraction of the total energy.

6.3 Scalar lepton decays via λ'_{ijk}

In the case of dominant λ'_{ijk} couplings, scalar leptons can decay indirectly as follows: $\tilde{\ell}_R \to \ell\,\tilde{\chi}^0_1 \to \ell\ell qq,\ \ell\nu qq$. The efficiencies for indirect decays are listed in Table 6. Only $\tilde{e}^+_R\tilde{e}^-_R$ pro-

duction has been considered. The efficiency is highest for large ΔM, when the two energetic electrons give a clear signature.

6.4 Scalar lepton decays via λ''_{ijk}

In the case of dominant λ''_{ijk} couplings, scalar leptons can decay indirectly as follows: $\tilde{\ell}_R \to \ell\,\tilde{\chi}^0_1 \to \ell qqq$. The efficiencies for indirect decays are listed in Table 6.

For scalar electron and muon decays, the efficiencies are highest for medium $\Delta M = M_{\tilde{\ell}_R} - M_{\tilde{\chi}^0_1}$ values, where events have high multiplicity satisfying the multijets selections and two energetic leptons which are well identified.

Supersymmetric partners of the right-handed leptons have no direct two-body decays via λ''_{ijk} couplings (see Table 1). However, when scalar leptons are lighter than $\tilde{\chi}^0_1$, the four-body [3] decay $\tilde{\ell}_R \to \ell qqq$ may occur. This provides the same final state ℓqqq resulting from indirect decays, but without internal $\tilde{\chi}^0_1$ resonance.

The non-resonant four-body decay is not implemented in the generator [10], which allows only scalar lepton decays via neutralino on-shell production. For this reason, we have used the results of the indirect decay analysis, performing a scan over all neutralino mass values between 0 GeV and $M_{\tilde{\ell}_R}$, for each value of $M_{\tilde{\ell}_R}$. The resulting lowest efficiency will be conservatively quoted in the following for four-body decays. It is found in most cases for $M_{\tilde{\chi}^0_1} \simeq M_{\tilde{\ell}_R}$, since in this case no isolated lepton can be identified. For scalar taus with masses above 70 GeV the lowest efficiency is found for high ΔM values, as in the case of indirect decays. Four-body decays are further discussed in Section 8.1.

7 Results

The summary of the searches is given in Tables 7 and 8, showing the number of candidates and expected background events. We do not observe any excess of events. Therefore we set upper limits on the neutralino, chargino and scala lepton production cross sections assuming direct or indirect R-parity violating decays. We also derive mass limits for these particles in the framework of the MSSM. Exclusion limits at 95% C.L. are derived taking into account the estimated background contamination. Systematic errors on the signal efficiency are evaluated as in Reference 22. The typical relative error is 5% and is dominated by Monte Carlo statistics. It is taken into account in the calculations of the signal upper limits [23].

7.1 Upper Limits on the Neutralino and Chargino Production Cross Sections

The 95% C.L. upper limits on neutralino and chargino pair-production cross sections at 189 GeV are shown in Figure 4.

In the case of dominant λ_{ijk} coupling, the neutralino pair-production cross section is below 0.2 pb at 95% C.L. for $M_{\tilde{\chi}^0_1} \geq 30$ GeV and below 0.1 pb for $M_{\tilde{\chi}^0_1} \geq 50$ GeV. The chargino cross section is below 0.3 pb for a chargino mass greater than 45 GeV in the direct R-parity violating decay mode and below 0.1 pb for $M_{\tilde{\chi}^\pm_1} = 94$ GeV and $\Delta M \leq 50$ GeV in the indirect decay mode.

When the λ'_{ijk} coupling is dominant, the neutralino cross section is below 0.5 pb at 95% C.L. for any value of the neutralino mass between 45 GeV and 94 GeV. The chargino cross

Direct decays		Mass values		
Coupling	Process	M = 5–20 GeV	M = 25–50 GeV	M=55–94 GeV
λ_{12k}	$\tilde{\ell}^+_R\tilde{\ell}^-_R$	–	–	8%–18%
λ_{121}	$\tilde{\nu}\bar{\tilde{\nu}}$	–	–	6%–8%
λ''_{212}	$\tilde{e}^+_R\tilde{e}^-_R$ *	–	32%–38%	35%–54%
λ''_{212}	$\tilde{\mu}^+_R\tilde{\mu}^-_R$ *	–	32%–38%	35%–54%
λ''_{212}	$\tilde{\tau}^+_R\tilde{\tau}^-_R$ *	–	32%–38%	15%–44%
Indirect decays		ΔM values		
Coupling	Process	ΔM = 5–20 GeV	ΔM = 25–50 GeV	ΔM = 55–80 GeV
λ_{133}	$\tilde{e}^+_R\tilde{e}^-_R$	74%–74%	50%–63%	26%–38%
λ_{133}	$\tilde{\mu}^+_R\tilde{\mu}^-_R$	82%–84%	76%–84%	65%–72%
λ_{133}	$\tilde{\tau}^+_R\tilde{\tau}^-_R$	66%–72%	67%–73%	57%–65%
λ_{133}	$\tilde{\nu}\bar{\tilde{\nu}}$	52%–52%	39%–49%	28%–37%
λ'_{311}	$\tilde{e}^+_R\tilde{e}^-_R$	30%–60%	50%–60%	60%–76%
λ''_{212}	$\tilde{e}^+_R\tilde{e}^-_R$	37%–63%	66%–69%	45%–62%
λ''_{212}	$\tilde{\mu}^+_R\tilde{\mu}^-_R$	29%–51%	54%–57%	34%–50%
λ''_{212}	$\tilde{\tau}^+_R\tilde{\tau}^-_R$	56%–66%	39%–62%	15%–16%

Table 6: Efficiency ranges at $\sqrt{s}$ = 189 GeV. Direct decays: the lowest mass value considered is $M_{\tilde{\ell}_R}$ = 54 GeV for λ_{12k}, $M_{\tilde{\nu}}$ = 54 GeV for λ_{121} and $M_{\tilde{\ell}_R}$ = 30 GeV for λ''_{212}. For the processes marked with * we refer to four-body decays, as described in Section 6.4. Indirect decays: the scalar lepton selection efficiencies correspond to $M_{\tilde{\ell}_R}$ $(M_{\tilde{\nu}})$ = 94 GeV.

Coupling	Process	$N_{background}$	N_{data}
λ_{ijk}	$\tilde{\chi}^0_1\tilde{\chi}^0_1$	2.0 ± 0.2	3
	$\tilde{\chi}^0_m\tilde{\chi}^0_n$	5.8 ± 0.4	5
	$\tilde{\chi}^+_1\tilde{\chi}^-_1$ (indirect)	3.8 ± 0.3	2
	$\tilde{\chi}^+_1\tilde{\chi}^-_1$ (direct)	20 ± 1	21
	$\tilde{\ell}^+_R\tilde{\ell}^-_R$ (direct)	18 ± 1	18
	$\tilde{\nu}\bar{\tilde{\nu}}$	5.8 ± 0.4	5
λ'_{ijk}	$\tilde{\chi}^0_1\tilde{\chi}^0_1$	77 ± 2	70
	$\tilde{\chi}^+_1\tilde{\chi}^-_1$	262 ± 2	257
	$\tilde{e}^+_R\tilde{e}^-_R$	26 ± 1	27
λ''_{ijk}	$\tilde{\chi}^0_1\tilde{\chi}^0_1$	357 ± 3	353
	$\tilde{\chi}^+_1\tilde{\chi}^-_1$	197 ± 1	193
	$\tilde{\ell}^+_R\tilde{\ell}^-_R$	154 ± 1	157

Table 7: Number of expected background and observed data events for the different processes. The same process (e.g. $\tilde{\chi}^+_1\tilde{\chi}^-_1$ direct decays via λ_{ijk}) can give rise to several topologies, or the same topology may occur in more than one final state. For this reason, details on the selection of each topology are given in Table 8. The error on the expected background is due to the limited Monte Carlo statistics.

Coupling	Selection	$N_{background}$	N_{data}
λ_{ijk}	$4\ell + \not{E}$	2.0 ± 0.2	3
	$(\geq 4)\ell +$ (jets) $+\not{E}$	3.8 ± 0.3	2
	$2\ell + \not{E}$	18 ± 1	18
	6ℓ	0.26 ± 0.05	0
λ'_{ijk}	4 jets $+\tau\tau$	30.0 ± 0.7	26
	4 jets $+\not{E}$	28.9 ± 0.8	31
	4 jets + τ + $\not{E}$	29.4 ± 1.2	25
	Multijets + lepton(s)	6.1 ± 0.2	8
	Multijets + $\not{E}$	65 ± 1	68
	Multijets + lepton(s) + $\not{E}$	11.7 ± 0.2	10
	Multijets	194 ± 1	187
λ''_{ijk}	$M_{\tilde{\chi}^0_1}$ = 20–30 GeV	47 ± 1	42
	$M_{\tilde{\chi}^0_1}$ = 30–40 GeV	79± 1	81
	$M_{\tilde{\chi}^0_1}$ = 40–50 GeV	48.1 ± 0.9	47
	$M_{\tilde{\chi}^0_1}$ = 50–60 GeV	98 ± 1	100
	Multijets	194 ± 1	187
	Semileptonic	1.6 ± 0.2	3
	Leptonic	3.2 ± 0.1	3
	Scalar leptons	154 ± 1	157

Table 8: Number of expected background and observed data events for the different selections (see Table 7). The error on the expected background is due to the limited Monte Carlo statistics.

section is below 0.5 pb for a chargino mass greater than 45 GeV in the direct decay mode and below 0.6 pb for $M_{\tilde{\chi}_1^\pm} = 94$ GeV and any value of ΔM in the indirect decay mode.

In the case of dominant λ''_{ijk} coupling, the neutralino cross section is below 0.35 pb at 95% C.L. for any value of the neutralino mass. The chargino cross section is below 0.35 pb for a chargino mass greater than 45 GeV in the direct decay mode and below 0.25 pb for $M_{\tilde{\chi}_1^\pm} = 94$ GeV and any value of ΔM in the indirect decay mode.

7.2 Upper Limits on the Scalar Lepton Production Cross Sections

The 95% C.L. upper limits on scalar lepton pair-production cross sections at 189 GeV are shown in Figure 5 and 6.

In the case of dominant λ_{ijk} coupling, the pair-production cross section for scalar charged leptons and scalar neutrinos is ≤ 0.5 pb for $M_{\tilde{\ell}_R}(M_{\tilde{\nu}}) \geq 70$ GeV, for direct decays. In the case of indirect R-parity violating decays, the upper limit on the cross section is between 0.050 pb and 0.100 pb for $M_{\tilde{\ell}_R}(M_{\tilde{\nu}}) = 94$ GeV and $\Delta M \leq 60$ GeV.

In the case of dominant λ'_{ijk} coupling, the pair-production cross section for scalar electrons directly decaying is ≤ 0.45 pb for any value of $M_{\tilde{\mathrm{e}}_\mathrm{R}} \geq 45$ GeV. In the case of $\tilde{e}_R$ indirect R-parity violating decays it is below 0.35 pb for any value of ΔM.

In the case of dominant λ''_{ijk} coupling, the pair-production cross section for scalar charged leptons directly decaying is ≤ 0.4 pb for any value of $M_{\tilde{\ell}_R}$. In the case of indirect R-parity violating decays, it is below 0.15 pb for scalar electrons and muons, for $M_{\tilde{\ell}_R} = 94$ GeV and $\Delta M \geq 10$ GeV. For scalar taus of 94 GeV it is below 0.4 pb for any value of ΔM.

8 Interpretation in the MSSM

The results are also interpreted as excluded regions in the MSSM parameter space. In the MSSM framework neutralino and chargino masses, couplings and cross sections depend on the gaugino mass parameter, M_2, the higgsino mass mixing parameter, μ, the ratio of the vacuum expectation values of the two Higgs doublets, $\tan\beta$, and the common mass of the scalar fermions at the GUT scale, m_0. Therefore the excluded regions can be expressed in the $M_2 - \mu$ plane for a given value of m_0 and $\tan\beta$. The results presented here hold for λ_{ijk}, λ'_{ijk} and $\lambda''_{ijk} > 10^{-5}$ and for $0 \leq M_2 \leq 1000$ GeV, -500 GeV $\leq \mu \leq 500$ GeV. They do not depend on the value of the trilinear coupling in the Higgs sector, A. A point in the MSSM parameter space is excluded if the total number of expected events is greater than the combined upper limit at 95% C.L. on the number of signal events. Neutralino, chargino and scalar lepton analyses are combined since several processes can occur at a given point.

In addition to the limits obtained with this analysis, we take into account the constraints from L3 cross section measurements at the Z pole. A point in the MSSM parameter space is excluded at 95% C.L. by Z lineshape measurements if:

$$\left(\frac{\sigma_{SUSY}}{\sigma_\mathrm{Z}}\right) \Gamma_\mathrm{Z} > \Gamma_{LIM}\,, \tag{4}$$

where σ_{SUSY} is the sum of the pair-production cross sections of supersymmetric particles at $\sqrt{s} = 91$ GeV, calculated with SUSYGEN [10], and σ_Z is the measured total Z cross section [21]. Γ_Z and $\Gamma_{LIM} = 22$ MeV are the measured total Z width and the 95% C.L. upper limit on possible non-Standard Model contributions to the total Z width [21].

Figures 7 and 8 show the excluded regions at 95% C.L. in the $M_2 - \mu$ plane for $\tan\beta = \sqrt{2}$ and $m_0 = 500$ GeV, and for $\tan\beta = 40$ and $m_0 = 70$ GeV. Moreover some regions beyond the chargino kinematic limit are excluded at large m_0 and low $\tan\beta$ values by the $\tilde{\chi}^0_m\tilde{\chi}^0_{n(n\geq 2)}$ analyses and at low m_0 by the $\tilde{\chi}^0_1\tilde{\chi}^0_1$ analyses.

8.1 Lightest scalar lepton $\tilde{\ell}_R$ as LSP

For $0 \leq m_0 < 50$ GeV and $1 \leq \tan\beta < 2$ the lightest scalar lepton, supersymmetric partner of the right-handed electron, can be the LSP. In this region, in the presence of dominant λ_{ijk} coupling the decay chain $\tilde{\chi}^0_1 \rightarrow \ell\tilde{\ell}_R \rightarrow \ell\ell\nu$ leads to the same final states arising from neutralino direct R-parity violating decays, so that the analysis is efficient also when the lightest scalar lepton is the LSP.

When the λ'_{ijk} or λ''_{ijk} couplings dominate, the decays $\tilde{\chi}^0_1 \rightarrow \ell\tilde{\ell}_R \rightarrow \ell\ell(\nu)qq$ or $\tilde{\chi}^0_1 \rightarrow \ell\tilde{\ell}_R \rightarrow \ell\ell qqq$ occur, respectively. Those five-body decays are not implemented in SUSYGEN [10]. However, since in this region $\tilde{\ell}_R$ is lighter than $\tilde{\chi}^0_1$, we can take into account the scalar lepton decays $\tilde{\ell}_R \rightarrow \ell(\nu)qq$ or $\tilde{\ell}_R \rightarrow \ell qqq$, as described in Sections 6.3 and 6.4.

8.2 Mass Limits

The results presented in this section hold for λ_{ijk}, λ'_{ijk} and $\lambda''_{ijk} > 10^{-5}$, $0 \leq M_2 \leq 1000$ GeV, -500 GeV $\leq \mu \leq 500$ GeV, $0 \leq m_0 \leq 500$ GeV and $0.7 \leq \tan\beta \leq 40$. All analysis contributions (neutralino, chargino and scalar lepton searches) are taken into account at the same time to derive the limits.

Figure 9 shows the 95% C.L. lower limits on neutralino and scalar lepton masses as a function of $\tan\beta$. The $\tilde{\chi}^0_1$ and $\tilde{\chi}^0_2$ limits are shown for $m_0 = 500$ GeV and the $\tilde{\ell}_R$ ones for $m_0 = 0$. At low m_0 ($m_0 \leq 70$ GeV), neutralino and slepton pair production are enhanced, allowing to get better results also at low values of $\tan\beta$. For high m_0 values those contributions are suppressed and the limit is given by the chargino exclusion. The absolute minimum on the slepton mass is found at $m_0 = 0$. For low m_0 values the different contributions depend on $\tan\beta$, since the $\tilde{\ell}_R$ can be the LSP for low $\tan\beta$ values ($\tan\beta < 2$) and therefore only scalar lepton analysis contribute to the limit in this region. For higher values of $\tan\beta$, $\tilde{\chi}^0_1$ is the LSP, and the lower limit on the scalar lepton mass is mainly given by $\tilde{\chi}^0_1\tilde{\chi}^0_1$ exclusion contours. As an example, Figure 10 shows the 95% C.L. lower limits on the mass of the supersymmetric partner of the right-handed electron for $\tan\beta = 2$.

The minima shown in Figure 9 correspond to the absolute minima from the complete scan on M_2, μ, m_0 and $\tan\beta$. The absolute limit on $M_{\tilde{\ell}_R}$ is found at $\tan\beta = 0.7$ in the case of λ_{ijk} and λ'_{ijk} and at $\tan\beta = 1.4$ for λ''_{ijk}. The difference is due to the better cross-section upper limit of λ''_{ijk} for scalar lepton direct decays (see Figure 5), since for λ_{ijk} and λ'_{ijk} the limit on $M_{\tilde{\ell}_R}$ is found when the $\tilde{\ell}_R$ is the LSP.

We derive lower limits at 95% C.L. on the neutralino, chargino and scalar lepton masses, as detailed in Table 9.

9 Updates at $\sqrt{s} = 192$–202 GeV

Only λ''_{ijk} analyses have been updated with 1999 data at $\sqrt{s} = 192$–202 GeV. Results of the different selections performed are shown in Table 10. No significant excess is seen. There is a

Particle Mass	λ_{ijk}	λ'_{ijk}	λ''_{ijk}
$M_{\tilde{\chi}_1^0}$	> 32.8 GeV	> 32.5 GeV	> 32.5 GeV
$M_{\tilde{\chi}_2^0}$	> 69.5 GeV	> 68.0 GeV	> 68.0 GeV
$M_{\tilde{\chi}_3^0}$	> 99.3 GeV	> 99.0 GeV	> 99.0 GeV
$M_{\tilde{\chi}_1^\pm}$	> 94.3 GeV	> 93.8 GeV	> 93.8 GeV
$M_{\tilde{\ell}_R}$	> 76.3 GeV	> 69.0 GeV	> 78.0 GeV
$M_{\tilde{\nu}}$	> 142.7 GeV	–	–

Table 9: Lower limits at 95% C.L. on the masses of the supersymmetric particles considered in this analysis. The limits on $M_{\tilde{\ell}_R}$ hold for $\tilde{e}_R$, $\tilde{\mu}_R$ and $\tilde{\tau}_R$.

slight deficit in the number of observed events, but within two standard deviations.

$\sqrt{s}$ (GeV)	192	196	200	202
$\int \mathcal{L}\ dt\ (pb^{-1})$	29.7	83.7	82.8	37.0
$\tilde{\chi}_1^0\tilde{\chi}_1^0 \to qqq\ qqq$ (N obs/N exp.)	43/47.6	107/128	116/122	50/55.8
$\tilde{\chi}_1^+\tilde{\chi}_1^- \to W^*\ W^*\ qqq\ qqq$	27/30.9	67/86.4	82/82.2	32/37.2
$\tilde{\ell}^+\tilde{\ell}^- \to \ell^+\ qqq\ \ell^-\ qqq$	26/27.7	62/77.7	82/74.0	30/34.9

Table 10: Results of the searches with λ''_{ijk} couplings in 192–202 GeVdata. The numbers quoted in this table are respectively the number of observed candidates and the number of expected events for the λ''_{ijk} selections.

The absence of significant excess has allowed to derive upper limits on the supersymmetric particle pair-production cross sections. Those limits are shown in Figure 11 as a function of the supersymmetric particle mass. The excluded cross–sections are between 50 fb and 600 fb for the combined data sample.

Performing a complete scan over m_0 and $\tan\beta$ as reported in Section 8 for 1998 data, we derive limits on the supersymmetric particle masses. The $\tilde{\chi}_1^0$ and $\tilde{\ell}_R$ mass limits as a function of $\tan\beta$ are shown in Figure 12 for several m_0 values.

From the complete scan over $0 \leq M_2 \leq 1000$ GeV, -500 GeV $\leq \mu \leq 500$ GeV, $0 \leq m_0 \leq 500$ GeV and $0.7 \leq \tan\beta \leq 40$, we set mass limits at 95% C.L. as detailed in Table 11.

SUSY particle	λ''
$\tilde{\chi}_1^0$	M>37.5 GeV
$\tilde{\chi}_2^0$	M>75.6 GeV
$\tilde{\chi}_1^\pm$	M>99.6 GeV
$\tilde{\ell}_R$	M> 86.0 GeV

Table 11: 95% C.L. lower limits on the supersymmetric particles masses, as obtained by the λ''_{ijk} analysis at $\sqrt{s}$ up to 202 GeV.

Acknowledgements

We wish to express our gratitude to the CERN accelerator divisions for the excellent performance of the LEP machine. We acknowledge the contributions of the engineers and technicians who have participated in the construction and maintenance of this experiment.

References

[1] A review can be found for example in:
H.E. Haber and G.L. Kane, Phys. Rep. **117** (1985) 75.

[2] C.S. Aulakh and R.N. Mohapatra, Phys. Lett. **B 119** (1982) 316;
F. Zwirner, Phys. Lett. **B 132** (1983) 103;
L.J. Hall and M. Suzuki, Nucl. Phys. **B 231** (1984) 419.
For a recent review and a reference to the literature:
H. Dreiner, "An introduction to explicit R-parity violation", hep–ph/9707435, published in *Perspectives on Supersymmetry*, ed. G.L. Kane, World Scientific, Singapore.

[3] R. Barbieri and A. Masiero, Nucl. Phys. **B 267** (1986) 679.

[4] S. Weinberg, Phys. Rev. **D 26** (1982) 287;
G. Bhattacharyya and P.B. Pal, "Upper bounds on all R-parity violating $\lambda\lambda''$ combinations from proton stability", hep–ph/9809493.

[5] Particle Data Group, C. Caso *et al.*, Eur. Phys. J. **C 3** (1998) 1.

[6] S. Dawson, Nucl. Phys. **B 261** (1985) 297.

[7] L3 Collab., M. Acciarri *et al.*, Phys. Lett. **B 459** (1999) 354.

[8] ALEPH Collab., D. Buskulic *et al.*, Phys. Lett. **B 349** (1995) 238;
ALEPH Collab., D. Buskulic *et al.*, Phys. Lett. **B 384** (1996) 461;
ALEPH Collab., R. Barate *et al.*, Eur. Phys. J. **C 4** (1998) 433;
ALEPH Collab., R. Barate *et al.*, Eur. Phys. J. **C 7** (1999) 383;
ALEPH Collab., R. Barate *et al.*, CERN-EP/99-093, subm. to Eur. Phys. J. **C**
OPAL Collab., G. Abbiendi *et al.*, Eur. Phys. J. **C 11** (1999) 619;
OPAL Collab., G. Abbiendi *et al.*, Eur. Phys. J. **C 12** (2000) 1;
DELPHI Collab., P. Abreu *et al.*, CERN-EP/99-049, subm. to Eur. Phys. J. **C**.

[9] L3 Collab., B. Adeva *et al.*, Nucl. Instr. and Meth. **A 289** (1990) 35;
J.A. Bakker *et al.*, Nucl. Instr. and Meth. **A 275** (1989) 81;
O. Adriani *et al.*, Nucl. Instr. and Meth. **A 302** (1991) 53;
B.Adeva *et al.*, Nucl. Instr. and Meth. **A 323** (1992) 109;
K. Deiters *et al.*, Nucl. Instr. and Meth. **A 323** (1992) 162;
M. Chemarin *et al.*, Nucl. Instr. and Meth. **A 349** (1994) 345;
M. Acciarri *et al.*, Nucl. Instr. and Meth. **A 351** (1994) 300;
G. Basti *et al.*, Nucl. Instr. and Meth. **A 374** (1996) 293;
I.C. Brock *et al.*, Nucl. Instr. and Meth. **A 381** (1996) 236;
A. Adam *et al.*, Nucl. Instr. and Meth. **A 383** (1996) 342.

[10] S. Katsanevas and S. Melachroinos, Proceedings of the Workshop "Physics at LEP 2", eds. G. Altarelli, T. Sjöstrand and F. Zwirner, CERN 96-01 (1996), vol. 2, p. 328.
`SUSYGEN 2.2`, S. Katsanevas and P. Morawitz, Comp. Phys. Comm. **112** (1998) 227.

[11] `PYTHIA 5.7` and `JETSET 7.4` Physics and Manual, T. Sjöstrand, CERN-TH/7112/93 (1993), revised August 1995; Comp. Phys. Comm. **82** (1994) 74.

[12] `BHWIDE`, S. Jadach *et al.*, Phys. Lett. **B 390** (1997) 298.

[13] `KORALZ:` Version 4.02 was used. S. Jardach, B.F.L. Ward, and Z. Wąs, Comp. Phys. Comm. **79** (1994) 503.

[14] `PHOJET:` Version 1.05 was used. R. Engel, Z. Phys. **C 66** (1995) 203;
R. Engel and J. Ranft, Phys. Rev. **D 54** (1996) 4244.

[15] `DIAG36:` F.A. Berends, P.H. Daverfeldt and R. Kleiss, Nucl. Phys. **B 253** (1985) 441.

[16] `KORALW:` Version 1.21 was used. M. Skrzypek, S. Jardach, W. Placzek, and Z. Wąs, Comp. Phys. Comm. **94** (1996) 216;
M. Skrzypek, S. Jardach, M. Martinez, W. Placzek, and Z. Wąs, Phys. Lett. **B 372** (1996) 289.

[17] `EXCALIBUR:` F.A. Berends, R. Kleiss and R. Pittau, Nucl. Phys. B 424 (1994) 308; Nucl. Phys. B 426 (1994) 344; Nucl. Phys. (Proc. Suppl.) B 37 (1994) 163; Phys. Lett. B 335 (1994) 490; Comp. Phys. Comm. 83 (1994) 141.

[18] `GEANT:` Version 3.15 was used. R. Brun et al, CERN DD/EE/84-1 (Revised 1987).

[19] H. Fesefeldt, RWTH Aachen Report PITHA 85/2 (1985).

[20] Yu. L. Dokshitzer, Contribution to the Workshop on Jets at LEP and HERA (1990);
N. Brown and W.J. Stirling, Rutherford Preprint RAL-91-049;
S. Catani *et al.*, Phys. Lett. **B 269** (1991) 432;
S. Bethke *et al.*, Nucl. Phys. **B 370** (1992) 310.

[21] L3 Collab., M. Acciarri *et al.*, "Measurements of Cross Sections and Forward-Backward Asymmetries at the Z Resonance and Determination of Electroweak Parameters", CERN-EP/2000-022, subm. to Eur. Phys. J. **C**.

[22] L3 Collab., M. Acciarri *et al.*, Phys. Lett. **B 377** (1996) 289.

[23] R.D. Cousins and V.L. Highland, Nucl. Instr. and. Meth. **A 320** (1992) 331.

[24] L3 Collab., M. Acciarri *et al.*, Phys. Lett. **B 472** (2000) 420.

λ_{ijk} : $4\ell + \not{E}$ selections				
	Low mass values ($\leq$ 25 GeV)		High mass values ($\geq$ 25 GeV)	
	$\ell = e, \mu$ only	$\ell = \tau$	$\ell = e, \mu$ only	$\ell = \tau$
$N_{e,\mu}$	≥ 2	–	≥ 2	–
$N_{e,\mu,\tau}$	–	≥ 3	–	≥ 3
N_{tracks}	4	4 – 6	3 – 4	3 – 8
$N_{clusters}$	4 – 8	4 – 16	4 – 8	6 – 24
N_{scint}	≥ 1	≥ 1	≥ 1	≥ 1
$E_{lum} + E_{alr}$ (GeV)	< 10	< 10	< 10	< 10
E_{bgo} (GeV)	< 150	> 20	< 100	–
E_{hcal} (GeV)	< 10	< 15	< 10	–
$E_{vis}/\sqrt{s}$	0.20 – 0.90	0.20 – 0.60	0.20 – 0.90	0.20 – 0.60
p_{miss} (GeV)	> 7	> 7	> 7	> 7
* $Thrust$	–	–	< 0.947	< 0.918
* $\sin(\theta_{miss})$	> 0.277	> 0.486	> 0.430	> 0.436
* θ_{acol} (rad)	< 3.107	< 3.135	< 3.035	< 2.952
* θ_{acop} (rad)	< 3.107	–	< 3.050	< 3.044
* y_{34}	0.0002 – 0.0018	0.0002 – 0.0020	> 0.00060	> 0.00056

Table 12: Cut values of the $4\ell + \not{E}$ selections, for final states with at least one τ or with $\ell = e, \mu$ only. Four lepton plus missing energy topologies result from neutralino, chargino and sneutrino decays, as detailed in Table 2. Different selection criteria are developed according to the mass values of the pair-produced supersymmetric particles. The variables are described in section 3. The cuts values of the variables marked with * are optimized simultaneously according to the procedure described in section 6.

λ_{ijk} : $2\ell + \not{E}$ and 6ℓ selections		
	$2\ell + \not{E}$	6ℓ
	$\ell = e, \mu, \tau$	$\ell = e, \mu, \tau$
$N_{e,\mu,\tau}$	= 2	≥ 4
N_{tracks}	2 – 4	5 – 11
$N_{clusters}$	3 – 5	6 – 18
N_{scint}	≥ 1	≥ 1
N_{jets8}	= 2	–
$E_{lum} + E_{alr}$ (GeV)	< 10	< 10
E_{bgo} (GeV)	–	15 – 125
E_1^{ℓ} (GeV)	30 – 60	–
$E_1^{\ell} + E_2^{\ell}$ (GeV)	> 40	–
$E_{vis}/\sqrt{s}$	0.25 – 0.55	0.30 – 1.20
p_{miss} (GeV)	> 7	> 7
* $Thrust$	–	< 0.971
* $\sin(\theta_{miss})$	> 0.278	> 0.314
* θ_{acol} (rad)	< 2.903	–
* θ_{acop} (rad)	< 2.904	–
* y_{34}	–	> 0.0009

Table 13: Cut values of the $2\ell + \not{E}$ and 6ℓ selections. Two lepton plus missing energy topologies result from chargino and slepton direct decays, as detailed in Table 2. Six leptons topologies arise from chargino direct decays. Inclusive selection criteria are developed for final states with $\ell = e, \mu$ or τ. The variables are descri bed in section 3. The cuts values of the variables marked with * are optimized simultaneously according to the procedure described in section 6.

λ_{ijk} : $(\geq 4)\ell +$ (jets) $+\not\!\!E$ selections, with $\ell = e, \mu$ only						
	$\Delta M \leq 20$ GeV	$\Delta M = 20 - 50$ GeV			$\Delta M \geq 50$ GeV		
$N_{e,\mu}$	≥ 2	≥ 2			≥ 2		
N_{scint}	≥ 1	≥ 1			≥ 1		
$E_{lum} + E_{alr}$ (GeV)	< 10	< 10			< 10		
E_{bgo} (GeV)	< 110	< 110			< 110		
p_{miss} (GeV)	> 7	> 7			> 7		
* $Thrust$	< 0.961	<0.878			<0.811		
* $\sin(\theta_{miss})$	> 0.259	> 0.362			> 0.389		
* θ_{acol} (rad)	< 3.044	< 3.112			< 2.998		
* θ_{acop} (rad)	< 3.139	< 3.136			< 3.065		
* y_{34}	> 0.0026	> 0.0109			> 0.0118		
		hadronic	mixed	leptonic	hadronic	mixed	leptonic
N_{tracks}	$5 - 11$	$12 - 26$	$8 - 17$	$5 - 8$	$18 - 28$	$8 - 22$	$5 - 6$
$N_{clusters}$	$6 - 26$	$35 - 52$	$18 - 40$	$6 - 12$	$38 - 60$	$20 - 42$	$6 - 11$
$E_{vis}/\sqrt{s}$	0.30–0.90	0.50–0.85	0.40–0.85	0.35–0.75	0.60–0.90	0.45–0.80	0.30–0.75

Table 14: Cut values of the $(\geq 4)\ell + (jets) + \not\!\!E$ selections, for final states with $\ell = e, \mu$ only. Multilepton plus possible jets and missing energies topologies result from neutralino, chargino and scalar lepton indirect decays, as detailed in Table 2. Different selection criteria are developed depending on the mass differences $\Delta M = M_{\tilde{\chi}^\pm_1} - M_{\tilde{\chi}^0_1}$, $M_{\tilde{\chi}^0_n} - M_{\tilde{\chi}^0_1}$ or $M_{\tilde{\ell}_R} - M_{\tilde{\chi}^0_1}$. For large and medium ΔM three selections are applied according to the W* decay channels in hadronic, mixed or leptonic final states. The variables are described in section 3. The cuts values of the variables marked with * are optimized simultaneously according to the procedure described in section 6.

λ_{ijk} : $(\geq 4)\ell +$ (jets) $+\not\!\!E$ selections, with $\ell = \tau$			
	$\Delta M \leq 20$ GeV	$\Delta M \geq 20$ GeV	
$N_{e,\mu,\tau}$	≥ 3	≥ 3	
N_{scint}	≥ 1	≥ 1	
$E_{lum} + E_{alr}$ (GeV)	< 10	< 10	
p_{miss} (GeV)	> 7	> 7	
* $Thrust$	< 0.991	<0.832	
* $\sin(\theta_{miss})$	> 0.396	> 0.464	
* θ_{acol} (rad)	< 3.058	< 3.092	
* θ_{acop} (rad)	–	< 3.140	
* y_{34}	> 0.0018	> 0.0141	
		hadronic and mixed	leptonic
N_{tracks}	$6 - 12$	$8 - 25$	$5 - 12$
$N_{clusters}$	$6 - 32$	$20 - 52$	$8 - 24$
$E_{vis}/\sqrt{s}$	0.30–0.65	0.30–0.70	0.30–0.70

Table 15: Cut values of the $(\geq 4)\ell + (jets) + \not\!\!E$ selections, for final states with at least one τ. Multilepton plus possible jets and missing energies topologies result from neutralino, chargino and scalar lepton indirect decays, as detailed in Table 2. Different selection criteria are developed depending on the mass differences $\Delta M = M_{\tilde{\chi}^\pm_1} - M_{\tilde{\chi}^0_1}$, $M_{\tilde{\chi}^0_n} - M_{\tilde{\chi}^0_1}$ or $M_{\tilde{\tau}_R} - M_{\tilde{\chi}^0_1}$. For ΔM larger than 20 GeV three selections are applied according to the W* decay channels in hadronic and mixed or leptonic final states. The variables are described in section 3. The cuts values of the variables marked with * are optimized simultaneously according to the procedure described in section 6.

λ'_{ijk} : 4j$\tau\tau$ selections			
	Low masses ($\leq$ 30 GeV)	Medium masses (35–50 GeV)	High masses ($\geq$ 55 GeV)
E_{v12}/E_{vis}	< 0.20		
$E_{lum} + E_{alr}$ (GeV)	< 1		
W mass window	reject if 70 GeV$< M_{qq} <$ 95 GeV and 70 GeV$< M_{\ell\nu} <$ 90 GeV		
N_{tracks}	8–29	5–34	13–38
$N_{clusters}$	16–63	24–73	43–94
N_{jet8}	–	–	≥ 4
$N_{e,\mu,\tau}$	≥ 1	≥ 1	≥ 2
$E_{miss}/\sqrt{s}$	< 0.33	< 0.35	< 0.24
$Prob(\chi^2_{WW}, 5)$	–	< 0.5	< 0.3
$Prob(\chi^2_{ZZ}, 5)$	–	–	< 0.3
$Sphericity$	0.003–0.3	< 0.42	0.1–0.81
W_{jet1}	0.04–0.36	≥ 0.1	≥ 0.1
W_{jet2}	0.04–0.36	≥ 0.1	–
$\lvert M_{jet1} - M_{jet2}\rvert$ (GeV)	<24	–	–
θ_{acol} (rad)	–	<3.09	–
$E_{bgo}/\sqrt{s}$	0.1–0.7	0.2–0.6	0.2–0.6
$E_{hcal}/\sqrt{s}$	0.05–0.4	0.05–0.3	0.05–0.35
* $Thrust$	0.94–0.99	0.83–0.98	0.61–0.83
* $\ln(y_{34})$	> -6.18	> -5.55	> -4.73
* $\sin(\theta_{miss})$	> 0.24	> 0.67	> 0.66
* $E_{vis}/\sqrt{s}$	0.59–0.89	0.67–0.95	0.69–0.88
* θ_{acop} (rad)	< 3.139	<3.093	< 3.136

Table 16: Details of final selections for the "4 jets + 2 taus" decay channel of the neutralinos for the λ' coupling, as detailed on Table 3. The variables are described in section 4. The cuts values of the variables marked with * are optimized simultaneously according to the procedure described in section 6.

λ'_{ijk} : 4j$\tau\nu$ selections			
	Low masses ($\leq$ 30 GeV)	Medium masses (35–50 GeV)	High masses ($\geq$ 55 GeV)
E_{v12}/E_{vis}	< 0.20		
$E_{lum} + E_{alr}$ (GeV)	< 1		
$N_{e,\mu,\tau}$	≥ 1		
W mass window	reject if 70 GeV$< M_{qq} <$ 95 GeV and 70 GeV$< M_{\ell\nu} <$ 90 GeV		
N_{tracks}	5–29	6–38	19–42
$N_{clusters}$	15–65	20–77	43–97
$E_{miss}/\sqrt{s}$	<0.37	<0.42	0.08–0.34
$Prob(\chi^2_W W, 5)$	<0.8	<0.16	<0.17
$Prob(\chi^2_Z Z, 5)$	<0.4	–	<0.5
$Sphericity$	<0.2	<0.46	0.08–0.8
W_{jet1}	0.03–0.4	0.04–0.65	≥ 0.2
W_{jet2}	0.03–0.5	0.04–0.65	≥ 0.05
$\lvert M_{jet1} - M_{jet2}\rvert$ (GeV)	<28	–	–
$E_{bgo}/\sqrt{s}$	0.1–0.66	0.13–0.66	0.21–0.56
$E_{hcal}/\sqrt{s}$	0.03–0.41	0.03–0.41	<0.40
* $Thrust$	0.95–0.99	0.84–0.99	0.60–0.85
* $\ln(y_{34})$	>-7.54	>-6.74	>-4.89
* $\sin(\theta_{miss})$	>0.35	>0.68	>0.47
* $E_{vis}/\sqrt{s}$	0.63–0.92	0.67–0.84	0.62–0.82
* θ_{acop} (rad)	<3.05	<3.02	–

Table 17: Details of final selections for the mixed decay channel of the neutralinos for the λ' coupling, as detailed on Table 3. The variables are described in section 4. The cuts values of the variables marked with * are optimized simultaneously according to the procedure described in section 6.

λ'_{ijk} : 4j$\nu\nu$ selections			
	Low masses ($\leq$ 30 GeV)	Medium masses (35–50 GeV)	High masses ($\geq$ 55 GeV)
E_{v12}/E_{vis}	$<$ 0.20		
$E_{lum}+E_{alr}$ (GeV)	$<$ 1		
N_{jet8}	–	–	≥ 3
$N_{e,\mu,\tau}$	≥ 1		
W mass window	reject if 70 GeV$< M_{qq} <$ 95 GeV and 70 GeV$< M_{\ell\nu} <$ 90 GeV		
N_{tracks}	4–31	6–33	14–41
$N_{clusters}$	10–64	18–74	43–99
$E_{miss}/\sqrt{s}$	<0.41	<0.41	0.08–0.43
$Prob(\chi^2_{WW},5)$	–	–	<0.1
Sphericity	<0.3	<0.52	0.05–0.78
W_{jet1}	0.02–0.4	0.04–0.65	$\geq$ 0.35
W_{jet2}	0.01–0.6	0.04–0.75	$\geq$ 0.07
$\lvert M_{jet1}-M_{jet2}\rvert$ (GeV)	<25	–	–
$E_{bgo}/\sqrt{s}$	0.08–0.57	0.11–0.57	0.11–0.57
$E_{hcal}/\sqrt{s}$	0.04–0.42	0.02–0.37	0.02–0.37
* *Thrust*	>0.95	0.91–0.97	0.55–0.92
* $\ln(y_{34})$	>-8.63	>-6.40	>-4.74
* $\sin(\theta_{miss})$	>0.66	>0.47	>0.62
* $E_{vis}/\sqrt{s}$	0.61–0.80	0.35–0.79	0.35–0.79
* θ_{acop} (rad)	<3.07	<3.05	<3.

Table 18: Details of final selections for the "4 jets + 2 neutrinos" decay channel of the neutralinos for the λ' coupling, as detailed on Table 3. The variables are described in section 4. The cuts values of the variables marked with * are optimized simultaneously according to the procedure described in section 6.

λ'_{ijk} : multijets + leptons selections			
$N_{clusters}$	≥ 13		
N_{tracks}	≥ 10		
E_{v12}/E_{vis}	$<$ 0.30		
$\sin(\theta_T)$	>0.139		
E_{par}/E_{vis}	<0.5		
E_{perp}/E_{vis}	<0.2		
N_{jets8}	≥ 3		
$E_{vis}/\sqrt{s}$	≥ 0.7		
$\sin(\theta_{miss})$	>0.139		
$N_{e,\mu}$	$\geq$ 2, one isolated ($E^{\ell}_{20}<$ 1GeV, $E_{lepton}>$ 5 GeV)		
$M_{\tilde{\chi}}$(GeV)	50	60	≥ 70
* *Thrust*	0.82–0.89	0.74–0.88	0.51–0.79
* $\ln(y_{34})$	>-5.56	>-5.22	> -5.80
* $\ln(y_{45})$	>-5.97	>-5.66	>-5.24

Table 19: Cut values for the first class of λ'_{ijk} charginos selections, with a multijet toplogy with at least 2 leptons and no missing energy as detailed in Table 3. Different selection criteria are developed according to the mass values of the pair–produced charginos. The variables are described in section 4. The cuts values of the variables marked with * are optimized simultaneously according to the procedure described in section 6.

λ'_{ijk} : multijets + $\not{E}$ selections			
$N_{clusters}$	≥ 13		
N_{tracks}	≥ 10		
E_{v12}/E_{vis}	$<$ 0.30		
$\sin(\theta_T)$	>0.139		
E_{par}/E_{vis}	<0.5		
E_{perp}/E_{vis}	<0.2		
N_{jets8}	≥ 3		
$E_{vis}/\sqrt{s}$	0.5–0.9		
$\sin(\theta_{miss})$	>0.436		
events with one lepton isolated ($E^{\ell}_{20}<$ 1 GeV) are rejected			
$M_{\tilde{\chi}}$(GeV)	50	60	≥ 70
* *Thrust*	0.82–0.90	0.71–0.84	0.54–0.80
* $\ln(y_{34})$	>-5.68	>-5.70	> -4.56
* $\ln(y_{45})$	>-6.17	>-5.94	>-5.21
* p_{miss}	> 10 GeV	> 20 GeV	> 20 GeV

Table 20: Cut values for the second class of λ'_{ijk} charginos selections, with a multijet topology with missing momentum and no isolated lepton, as detailed in Table 3. Different selection criteria are developed according to the mass values of the pair–produced charginos. The variables are described in section 4. The cuts values of the variables marked with * are optimized simultaneously according to the procedure described in section 6.

λ'_{ijk} : multijet + lepton(s) and $\not{E}$ selection	
$N_{clusters}$	≥ 13
N_{tracks}	≥ 10
E_{v12}/E_{vis}	< 0.30
$\sin(\theta_T)$	>0.139
E_{par}/E_{vis}	<0.5
E_{perp}/E_{vis}	<0.2
N_{jets8}	≥ 3
$E_{vis}/\sqrt{s}$	<0.9
$\sin(\theta_{miss})$	>0.436
$N_{e,\mu}$	≥ 1, one isolated ($E_{20}^{\ell} < 1$ GeV, $E_{lepton} < 30$ GeV)
W mass window	reject if 70 GeV< M_{qq} < 90 GeV and 70 GeV< $M_{\ell\nu}$ < 90 GeV
* $Thrust$	0.56–0.87
* $\ln(y_{34})$	> -5.35
* $\ln(y_{45})$	> -6.22
* p_{miss}	> 12.3 GeV

Table 21: Cut values for the third class of λ'_{ijk} charginos selections, with a multijet topology with both lepton(s) and missing energy. The variables are described in section 4. The cuts values of the variables marked with * are optimized simultaneously according to the procedure described in section 6.

λ'_{ijk} : scalar electron selections	
$N_{clusters}$	≥ 13
N_{tracks}	≥ 1
$E_{vis}/\sqrt{s}$	> 0.70
E_{perp}/E_{vis}	< 0.20
E_{par}/E_{vis}	< 0.20
E_{v12}/E_{vis}	< 0.30
E_{bgo}/E_{vis}	0.05 – 0.98
$\sqrt{s'}/\sqrt{s}$	> 0.80
$\sin(\theta_T)$	> 0.139
$Thrust$	< 0.95
$\ln(y_{34})$	> -8.0
$\ln(y_{45})$	> -9.0
N_e	≥ 1
E_1^{ℓ} (GeV)	> 5

Table 22: Cuts values of the slepton selections, for final states with 6 jets and 2 leptons, as detailed in Table 3. The variables are described in section 4. The cuts values of the variables marked with * are optimized simultaneously according to the procedure described in section 6.

λ''_{ijk} : multijet selections					
$N_{clusters}$	≥ 13				
N_{tracks}	≥ 1				
$E_{vis}/\sqrt{s}$	> 0.70				
E_{perp}/E_{vis}	< 0.20				
E_{par}/E_{vis}	< 0.20				
E_{v12}/E_{vis}	< 0.30				
E_{bgo}/E_{vis}	0.05 – 0.98				
$\sqrt{s'}/\sqrt{s}$	> 0.80				
$\sin(\theta_T)$	> 0.139				
$M_{\tilde{\chi}}$(GeV)	20 – 30	30 – 40	40 – 50	50 – 60	≥ 60
* $Thrust$	0.940 – 0.973	0.901 – 0.960	0.828 – 0.919	0.755 – 0.889	0.575 – 0.844
* $\ln(y_{34})$	> -5.85	> -5.70	> -5.20	> -5.16	> -4.77
* $\ln(y_{45})$	> -9.68	> -7.02	> -6.16	> -5.82	> -4.62
* W_{jet1}	0.12 – 0.22	0.15 – 0.45	0.25 – 0.55	0.21 – 0.67	0.38 – 0.90

Table 23: Cut values of the neutralino selections, for final states with at least six hadronic jets. The same multijet topologies arise from indirect neutralino and chargino hadronic decays, as detailed in Table 4. Different selection criteria are developed according to the mass values of the pair-produced supersymmetric particles. The variables are described in section 5. The cuts values of the variables marked with * are optimized simultaneously according to the procedure described in section 6.

λ''_{ijk} : multijet + leptons selections		
$N_{clusters}$	≥ 13	
E_{v12}/E_{vis}	< 0.20	
E_{bgo}/E_{vis}	0.05–0.98	
$\sin(\theta_T)$	>0.139	
	semileptonic	leptonic
E_{par}/E_{vis}	< 0.3	< 0.5
E_{perp}/E_{vis}	< 0.3	< 0.5
N_{tracks}	> 20	10–30
$N_{e,\mu,\tau}$	≥ 1	≥ 2
E_{20}^{ℓ}	> 1 GeV	–
* $Thrust$	0.52–0.83	0.55–0.79
* $\ln(y_{34})$	> -4.55	> -4.15
* $\ln(y_{45})$	> -5.02	> -4.58
* $\sin(\theta_{miss})$	> 0.24	> 0.51
* $E_{vis}/\sqrt{s}$	> 0.6	0.52–0.88

Table 24: Details of final selections for semileptonic and leptonic decays channels of the charginos for the λ'' coupling, as detailed on Table 4. The variables are described in section 5. The cuts values of the variables marked with * are optimized simultaneously according to the procedure described in section 6.

λ''_{ijk} : slepton selections			
Corresponding Neutralino selection cuts (for $M_{\tilde{\chi}_1^0} \equiv M_{\tilde{\ell}}$) +			
Selectron	Smuon	Stau	Stau High ΔM
2 electrons	2 muons	1 lepton $(e, \mu, \tau\ )$	
For at least one of them: $E_{20}^{\ell} > 1$ GeV		–	$M_{5C} = M_{\tilde{\tau}} \pm 5$ GeV.

Table 25: Cuts values of the slepton selections, for final states with 6 jets and 2 leptons, as detailed in Table 4. Different selection criteria are developed according to the lepton flavour expected in the final state. The variables are described in section 5. The cuts values of the variables marked with * are optimized simultaneously according to the procedure described in section 6.

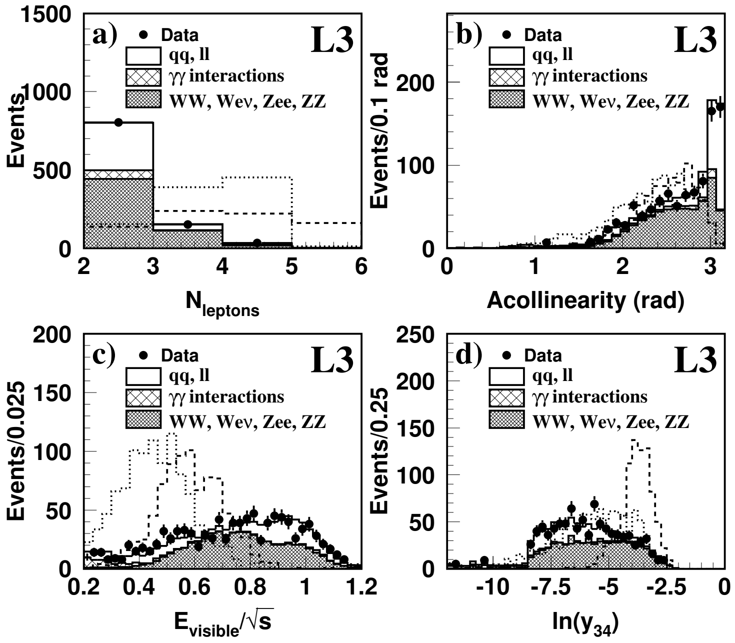

Figure 1: Distributions of a) the number of leptons, b) acollinearity, c) the normalised visible energy and d) $\ln(y_{34})$ after the λ_{ijk} preselection. The solid histograms show the expectations for Standard Model processes at $\sqrt{s} = 189$ GeV. The dotted and dashed histograms show two examples of signal, with dominant coupling λ_{133}. The dotted histograms represent the process $e^+e^- \to \tilde{\chi}_1^0\tilde{\chi}_1^0$, for $M_{\tilde{\chi}_1^0} = 94$ GeV. The dashed ones represent $e^+e^- \to \tilde{\chi}_1^+\tilde{\chi}_1^-$, with $M_{\tilde{\chi}_1^\pm} = 94$ GeV and $\Delta M = 40$ GeV.

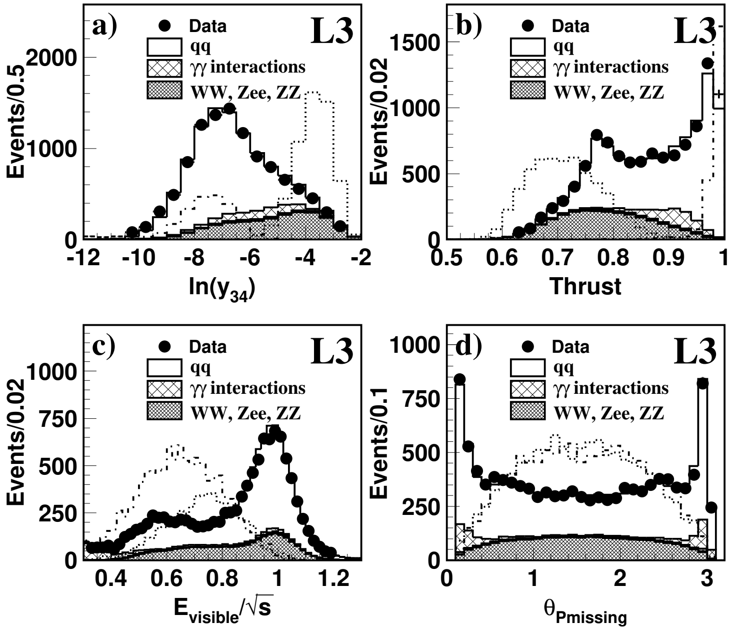

Figure 2: Distributions of a) $\ln(y_{34})$, b) thrust, c) normalised visible energy and d) polar angle of the missing momentum after the λ'_{ijk} preselection. The solid histograms show the expectations for Standard Model processes at $\sqrt{s} = 189$ GeV. The dashed and dotted histograms show two examples of signal. The dashed histograms represent the process $e^+e^- \to \tilde{\chi}^0_1\tilde{\chi}^0_1 \to 4$ jets $\nu\bar{\nu}$, with $M_{\tilde{\chi}^0_1} = 15$ GeV. The dotted ones represent $e^+e^- \to \tilde{\chi}^+_1\tilde{\chi}^-_1$, with $M_{\tilde{\chi}^\pm_1} = 94$ GeV and $\Delta M = 55$ GeV, with subsequent $\tilde{\chi}^0_1\tilde{\chi}^0_1$ decays into 4 jets $\nu\bar{\nu}$.

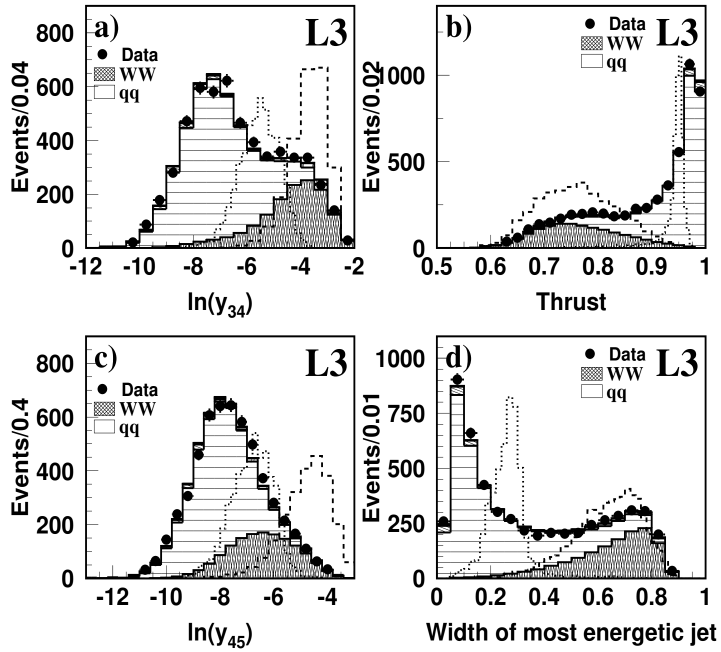

Figure 3: Distributions of a) $\ln(y_{34})$, b) thrust, c) $\ln(y_{45})$ and d) width of the most energetic jet after the λ''_{ijk} preselection. The solid histograms show the expectations for Standard Model processes at $\sqrt{s} = 189$ GeV. The dashed and dotted histograms show two examples of signal, with dominant coupling λ''_{212}. The dashed histograms represent the process $e^+e^- \to \tilde{\chi}^0_1\tilde{\chi}^0_1$, with $M_{\tilde{\chi}^0_1} = 94$ GeV. The dotted ones represent the same process, with $M_{\tilde{\chi}^0_1} = 30$ GeV.

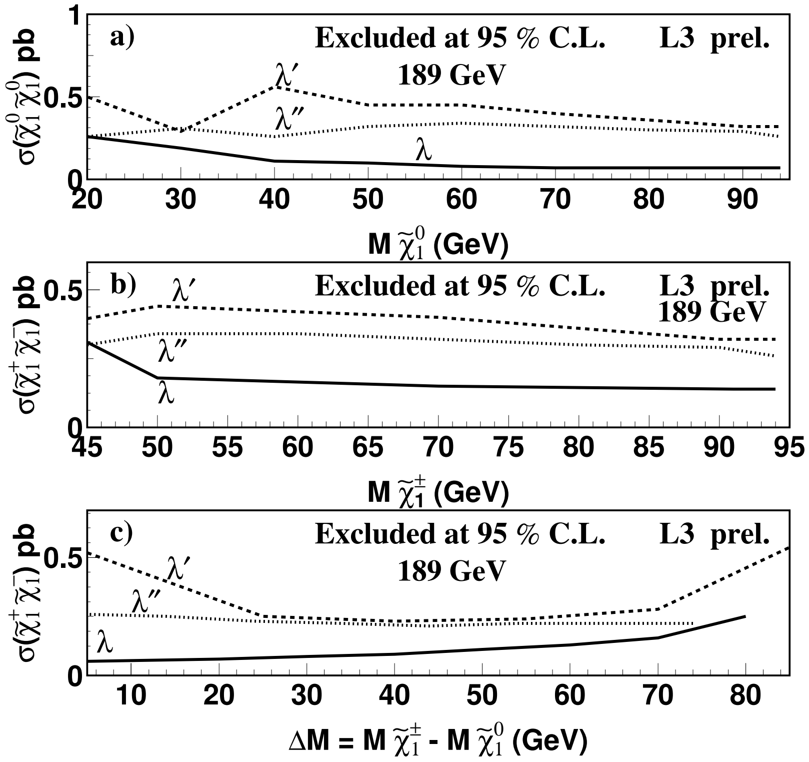

Figure 4: 95% C.L. upper limits on: a) the neutralino production cross section as a function of the neutralino mass, b) the chargino production cross section as a function of the chargino mass, in the direct decay mode and c) the chargino production cross section as a function of ΔM, for $M_{\tilde{\chi}_1^\pm} = 94$ GeV, in the indirect decay mode. The solid lines show the limits obtained by the $\lambda_{ijk} = \lambda_{133}$ analysis, the dotted lines show those obtained by the $\lambda'_{ijk} = \lambda'_{311}$ analysis and the dashed lines show those obtained by the $\lambda''_{ijk} = \lambda''_{212}$ analysis.

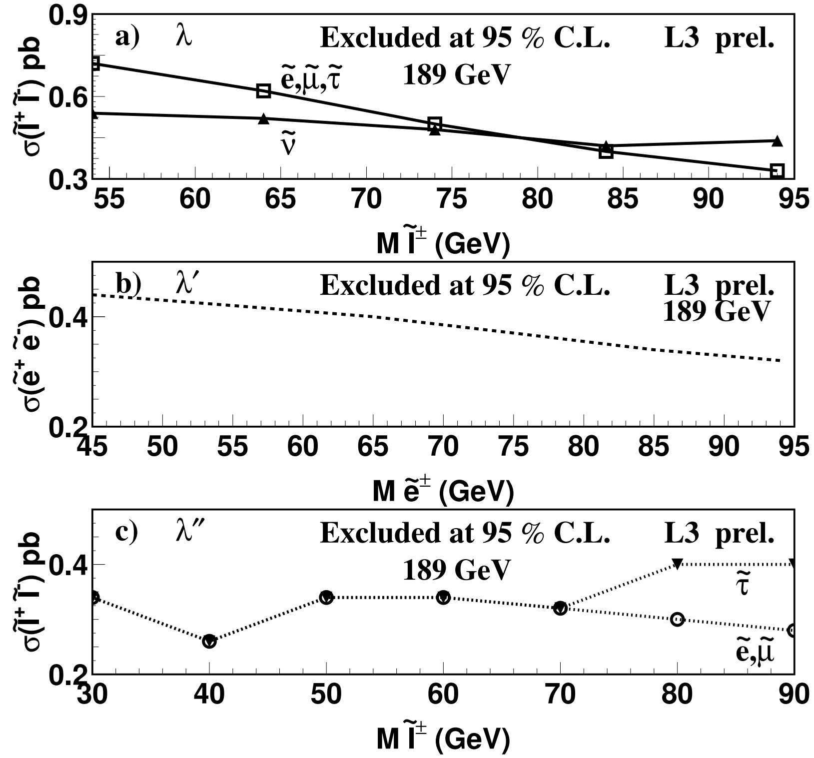

Figure 5: 95% C.L. upper limits on the scalar lepton production cross section, in the direct decay mode, as a function of the scalar lepton mass for: a) λ_{ijk}, b) λ'_{ijk} and c) λ''_{ijk}. The solid lines show the limits obtained by the $\lambda_{ijk} = \lambda_{12k}$ analysis for scalar electrons, muons and taus and by the $\lambda_{ijk} = \lambda_{121}$ analysis for scalar neutrinos. The dashed line show the limit obtained by the $\lambda'_{ijk} = \lambda'_{311}$ analysis for scalar electrons. The dotted lines show those obtained by the $\lambda''_{ijk} = \lambda''_{212}$ analysis for scalar electrons, muons and taus.

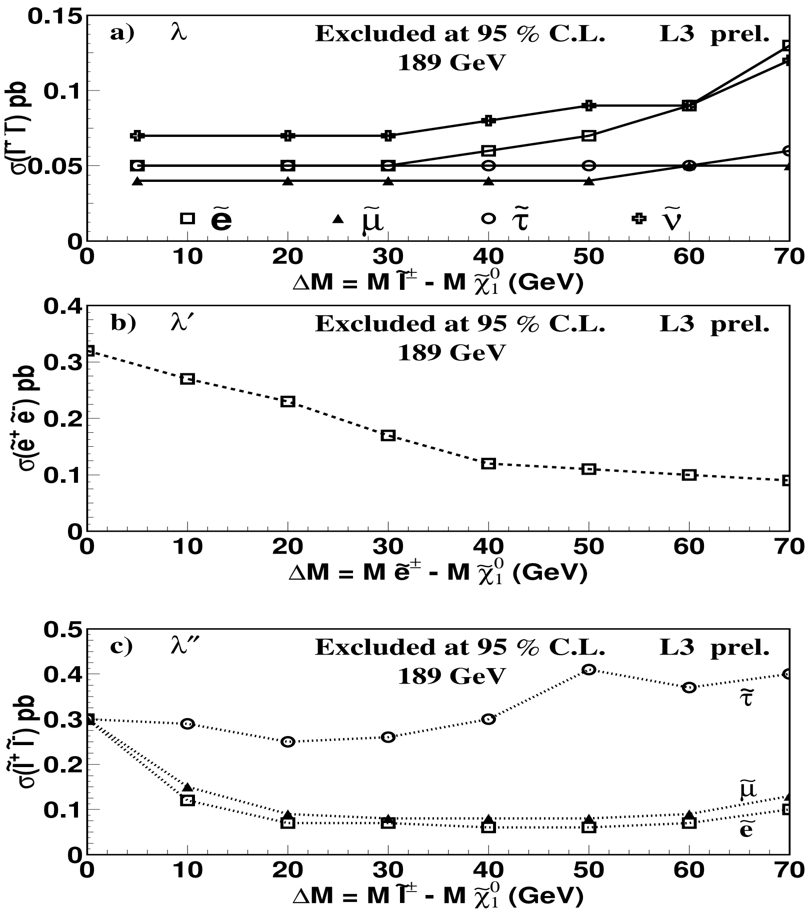

Figure 6: 95% C.L. upper limits on the scalar lepton production cross section, in the indirect decay mode, for $M_{\tilde{\ell}_R} = 94$ GeV and as a function of ΔM, for: a) λ_{ijk} and b) λ''_{ijk}. The solid lines show the limits obtained by the $\lambda_{ijk} = \lambda_{133}$ analysis for scalar electrons, muons, taus and neutrinos. The dashed line show the limit obtained by the $\lambda'_{ijk} = \lambda'_{311}$ analysis for scalar electrons. The dotted lines show those obtained by the $\lambda''_{ijk} = \lambda''_{212}$ analysis for scalar electrons, muons and taus.

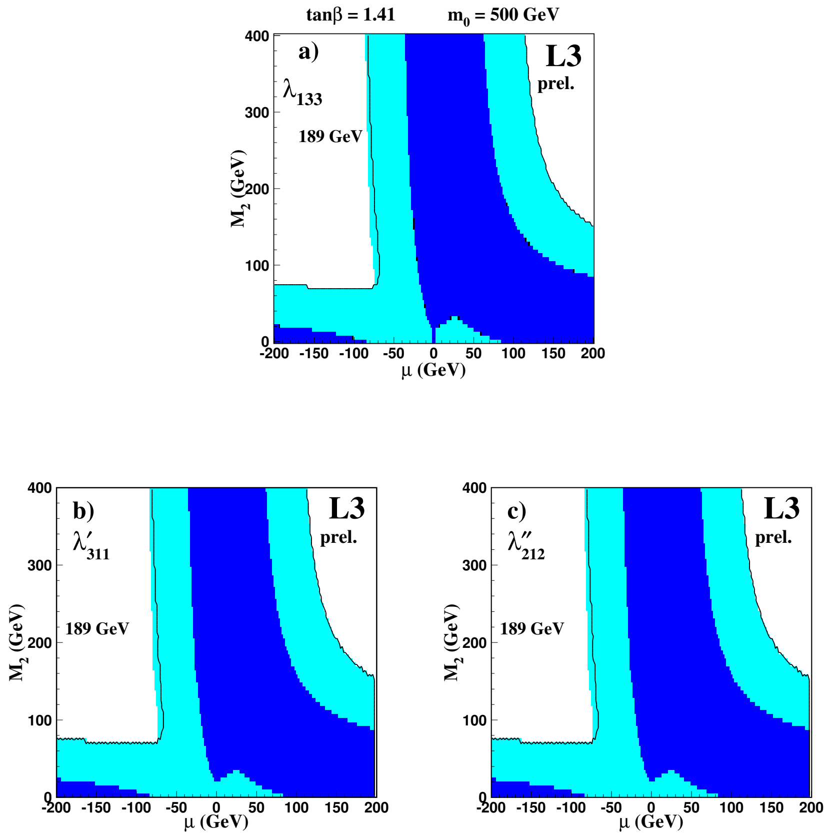

Figure 7: Exclusion regions at 95% confidence level for $\lambda_{ijk} = \lambda_{133}$ (a), $\lambda'_{ijk} = \lambda'_{311}$ (b) and $\lambda''_{ijk} = \lambda''_{212}$ (c), for $\tan\beta = \sqrt{2}$ and $m_0 = 500$ GeV. The dark grey region is excluded by the Z lineshape measurements and the light grey region by the present analyses. The black solid lines indicate the chargino kinematic limit. The grey region beyond the kinematic limit is excluded by neutralino analyses.

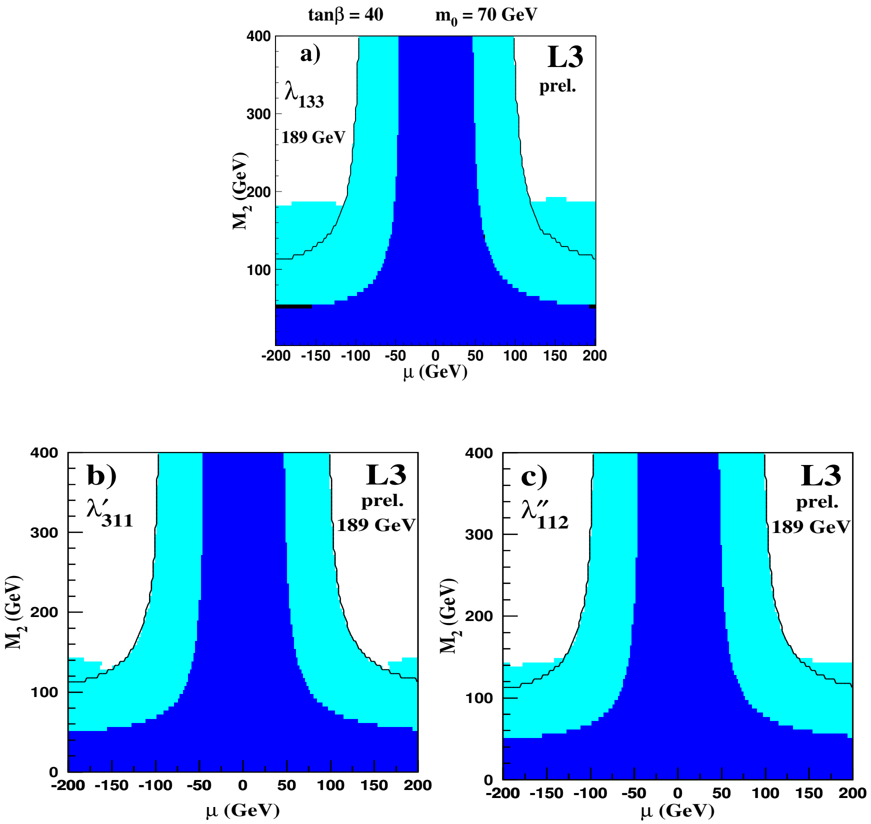

Figure 8: Exclusion regions at 95% confidence level for $\lambda_{ijk} = \lambda_{133}$ (a), $\lambda'_{ijk} = \lambda'_{311}$ (b) and $\lambda''_{ijk} = \lambda''_{212}$ (c), for $\tan\beta = 40$ and $m_0 = 70$ GeV. The dark grey region is excluded by the Z lineshape measurements and the light grey region by the present analyses. The black solid lines indicate the chargino kinematic limit. The grey region beyond the kinematic limit is excluded by neutralino analyses.

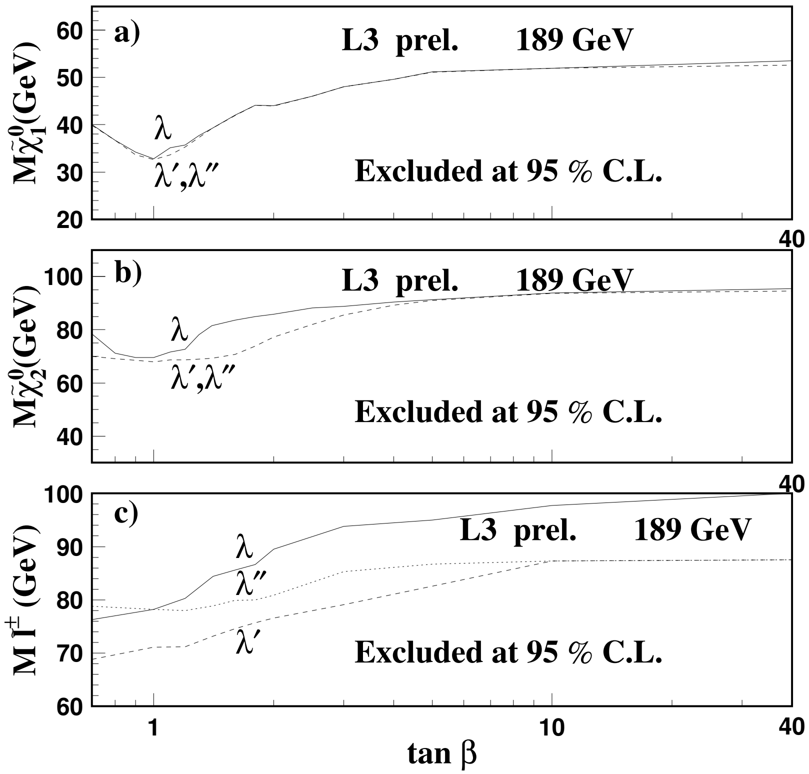

Figure 9: 95% C.L. lower limits on the masses of $\tilde{\chi}^0_1$ (a), $\tilde{\chi}^0_2$ (b) and $\tilde{\ell}_R$, as a function of $\tan\beta$, for $0 \leq M_2 \leq 1000$ GeVand -500 GeV $\leq \mu \leq 500$ GeV. m_0 is fixed and equal to 500 GeV in (a) and (b) and $m_0 = 0$ in (c).

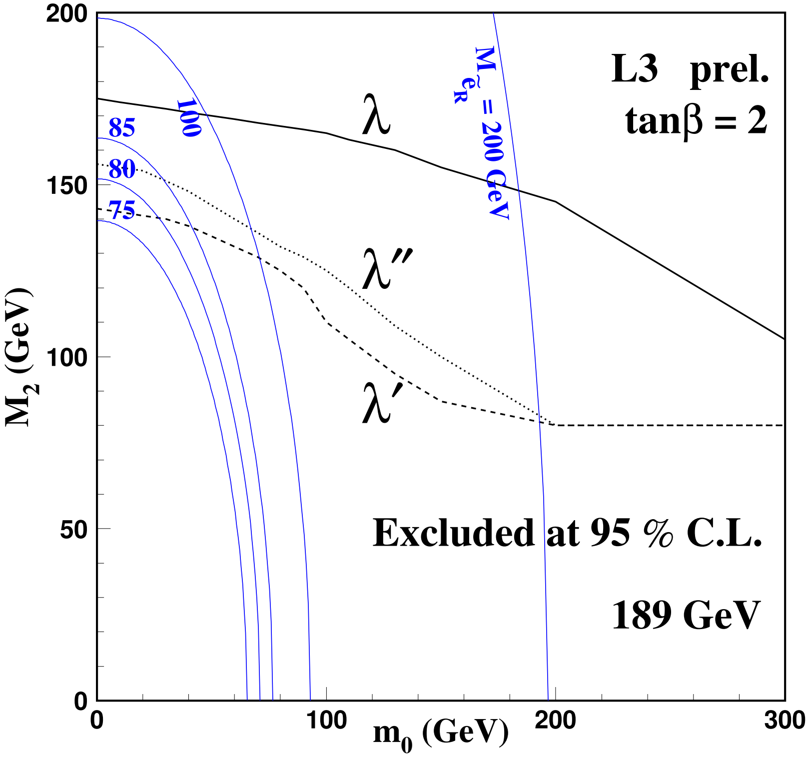

Figure 10: 95% C.L. exclusion contours in the $M_2 - m_0$ plane, for $\tan\beta = 2$ and $\mu < 0$. The lines labelled with the corresponding value in GeV represent the contours of constant scalar electron mass $M_{\tilde{e}_R}$. The solid, dotted and dashed curves show the 95% C.L. lower limits on M_2 as a function of m_0. The contribution from scalar lepton, neutrlino and chargino searches is included.

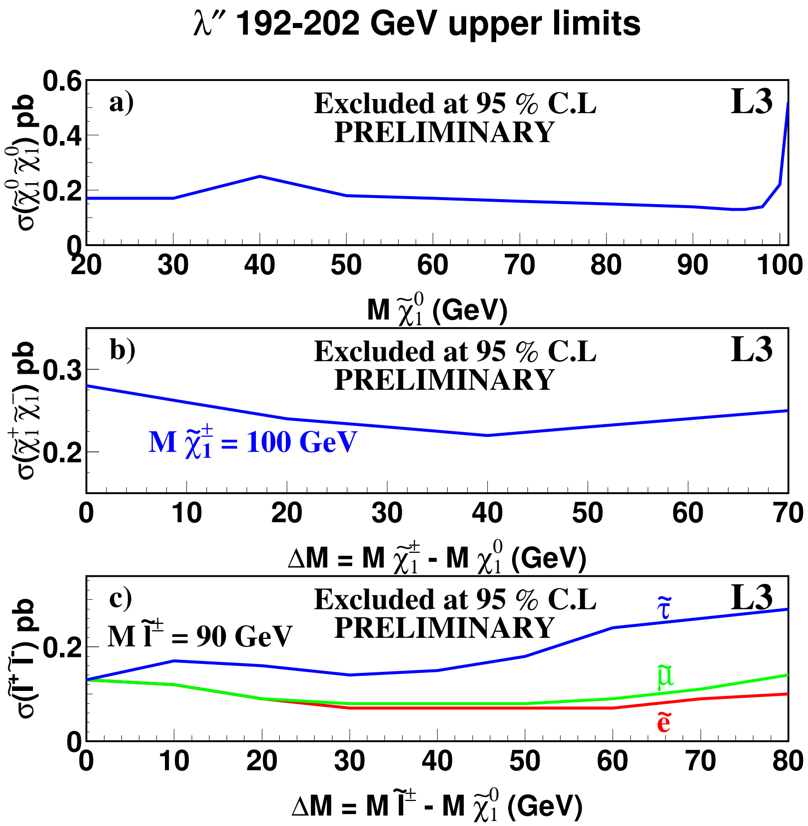

Figure 11: Excluded cross–sections for: a) $\tilde{\chi}^0_1\,\tilde{\chi}^0_1$ decays as a function of $\tilde{\chi}^0_1$ mass b) $\tilde{\chi}^+_1\,\tilde{\chi}^-_1$ decays as a function of $\tilde{\chi}^0_1$ mass, for a fixed $\tilde{\chi}^\pm_1$ mass of 100 GeV c) $\tilde{\ell}^+\tilde{\ell}^-$ decays as a function of $\tilde{\chi}^0_1$ mass for a $\tilde{\ell}$ mass of 90 GeV ($\tilde{\ell} = \tilde{e},\ \tilde{\mu},$ or $\tilde{\tau}$)

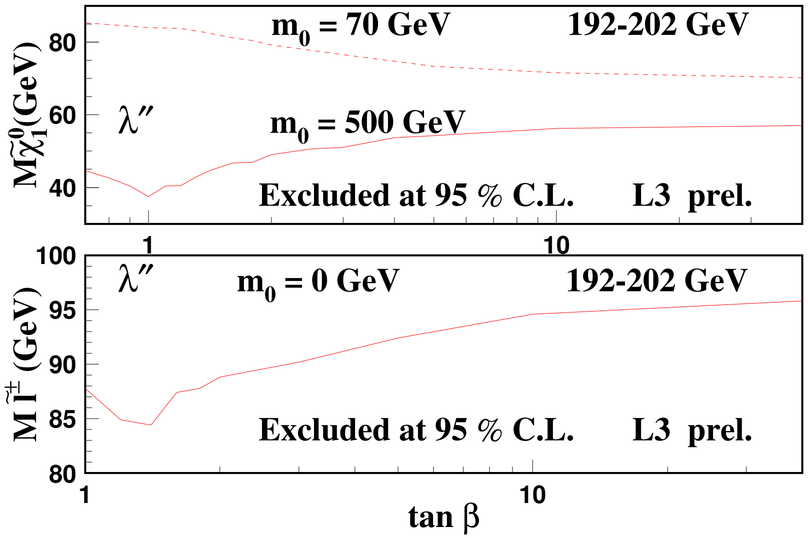

Figure 12: 95% C.L. lower limit on the masses of $\tilde{\chi}^0_1$ (a) and $\tilde{\ell}_R$ (b) as a function of $\tan\beta$ for given values of m_0 .